CLM-P572

CLM-P572

UKAEA

Preprint

HELIUM COOLING CIRCUITS FOR A FUSION REACTOR

R A W SHOCK

CULHAM LABORATORY
Abingdon Oxfordshire

1979

CLM-P572

HELIUM COOLING CIRCUITS FOR A FUSION REACTOR

R. A. W. SHOCK*

Culham Laboratory, Abingdon, Oxon, OX14 3DB, UK.

(Euratom/UKAEA Fusion Association)

A B S T R A C T

A thermal and hydraulic analysis of the complete cooling circuit of a helium cooled fusion reactor is presented. The study is based on the Culham Conceptual Tokamak Reactor Mark II but seeks to be as general as possible.

Mathematical techniques have been devised to model complex ducting networks. To begin with these are applied to rows of blanket cells. It is shown that ducting diameters must be of the order of 0.15m or greater. If the ducts are too small not only is the pressure drop too great but some blanket cells are overcooled at the expense of others which overheat.

The complete system consisting of many rows of cells and the inter-connecting ductwork, together with pumps and heat exchangers, is then analysed. Design option regions are drawn for a variety of operating parameters. These regions are bounded by criteria such as maximum pumping power fraction, minimum economic wall loading, minimum thermodynamic efficiency and maximum temperature. Because the maximum operating temperature depends not only on pressure and duct sizes but also on the material of construction, different regions can be drawn for different materials. The size of the region, and with it the maximum wall loading, decreases as the pressure and the coolant ducting diameter decrease. For the three candidate materials examined it is largest for TZM, smallest for stainless steel and intermediate for Inconel 718.

(Submitted for publication in Nuclear Engineering and Design)

* AERE Harwell

February 1979

1. INTRODUCTION

In first generation fusion reactor power stations the tritium fuel will be bred by the reaction between neutrons and lithium atoms in a blanket surrounding the plasma. Since the thermal conductivity of liquid metals is relatively high it would seem an attractive proposition to use liquid lithium both as the coolant and as the tritium source. This concept has been studied by Hunt and Hancox (1). The use of boiling water as the coolant would simplify the plant involved (as for BWR and SGHWR) but has not yet been studied in depth.

A third possible class of coolants is gases, in particular carbon dioxide and helium for both of which there is considerable experience in the nuclear field. Of the two, helium has a number of advantages (2), the most important being its higher thermal conductivity and specific heat and its lower corrosiveness; its main disadvantage being cost. It is quite possible that helium will be chosen as the coolant for the first commercial fusion reactor based power stations, as it has been for such conceptual designs as UWMAK and CCTR (Culham Conceptual Tokamak Reactor).

This work presents a thermal and hydraulic analysis of the complete cooling circuit of a fusion reactor system. Many configurations of reactor, such as mirror, reversed fuel pinch and tokamaks, have been proposed; this work is concerned exclusively with the last. Although the possibility of a closed cycle operation involving only helium has been discussed (3) this study assumes a conventional steam raising system. On leaving the helium/steam heat exchangers the coolant gas enters the reactor where it is distributed through a suitable manifolding system to the blanket cells. At exit it is similarly collected and pumped to the helium/steam heat exchangers.

Several conceptual designs of gas cooled blanket cells have been proposed (4) and (5) and the pressure and temperature distributions within these cells have been analysed. No such attention has yet been paid to the flow in the complex manifolding and ducting which join the cells, nor to their interaction with the parts of the circuit external to the reactor and it is those areas which are the subject of the present study. We examine the effect on the overall pumping power of inter-connecting ductwork sizes, of coolant inlet temperature and temperature rise, of maximum allowable stresses and of operating pressure. This study seeks to be as general as possible, but for calculations take as a sample system the Culham Conceptual Tokamak Reactor Mark II. This exists in two versions, CCTR-II-A and II-B. The former envisages separated coolant feed and removal ducting system, the latter a concentric system. In this study the layout of the former is considered combined with the torus geometry, power output and wall loading of the less optimistic CCTR-II-B.

Figure 1 shows the CCTR-II-A. A description of the concept is given by Mitchell and Hollis (6) but those parts which concern the present study are summarised in detail. The torus is made up of 20 segments (slices of the "doughnut" when viewed from above). The cooling system of each segment consists primarily of rows of blanket cells stacked around the minor circumference of the torus. The manifolding of the cells is such that rows of them, in the horizontal plane, have common coolant feed and return lines. In the latest concept the top and bottom half of each segment will be piped independently. The main coolant supply duct (region 5 in Figure 1) will follow the minor circumference of the torus with offshoot pipes branching to feed the rows of blanket cells. Each offshoot pipe feeds a manifold running along the back of a cell row from which supply pipes run to the individual blanket cells. The diameter of the main coolant supply

duct decreases progressively around the minor circumference as the flowrate in it diminishes. Similar, side-by-side arrangements will exist for the supply and removal of the coolant. Figure 2 shows a layout drawing of the network of pipes for the supply, or removal, of the helium in the half segments. The more recent concept, a concentric piping system with the main feed and return pipes at the bottom only is briefly discussed in section 5.

Periodically, it will be necessary, due to neutron damage, to renew the structure of the blanket cells. This will necessitate a number of remotely controlled operations which include pipe cutting and welding and segment movement. Mitchell and Hollis (6) discuss the impact of the servicing requirements on the design.

The blanket cells considered here are based largely on the conceptual design study by Mitchell and Booth (4), see Figure 3. In this design entering coolant flows directly to the centre of the front wall, i.e. to the region of greatest heat release. The coolant then splits into eight streams. Four pipes are attached to, and cool, the sidewalls and four spiral back through the bulk of the lithium. Mitchell and Booth give relationships for the pressure loss in a blanket cell and for the temperature difference between the coolant tube walls and the bulk gas.

In the present study the calculation method follows the hierarchical structure of the system. The simplest unit, the blanket cell, has, as described, already been analysed by Mitchell and Booth (4) although some further considerations necessary for this study are noted, see section 2. Groups of three, four or five such units are manifolded together with common feed and return pipes and such cell rows are the subject of section 3. The group of cell rows round half the circumference, manifolded together as in Figure 2, are then similarly treated in section 4, drawing on the results of the previous section. The half segments can be linked to the steam raisers in a number of possible ways; the number of heat exchanger/compressor units could theoretically vary between one for each half segment (40 for CCTR-II) and one for the complete reactor. In the present study it is envisaged that pairs of half segments (those forming complete segments) will be linked to a common heat exchanger and compressor. Section 4 also examines such units. Finally section 5 presents the conclusions from the complete study.

2. BLANKET CELLS

The blanket cell design is that proposed by Mitchell and Booth (4), see Figure 3; the analysis is extended to consider pressure limitations imposed by the external circuit. They showed that the pressure loss is given by:

$$\Delta P = \tfrac{1}{2}\left[\frac{4m}{\pi d_i^2}\right]^2 \frac{\Psi}{d_i}\,\frac{RL}{P}\,\bar{T} \qquad (1)$$

It was assumed that the flow through all the eight internal ducts would be identical: in fact the flows will be self adjusting such that the pressure drop in each type of duct (wall and bulk) will be equal. For the present purposes equation (1) is used with m given by the average value.

The mean temperature of the gas ($= T_{in} + \Delta T/2$) depends on the inlet temperature and temperature rise. To maximise the thermodynamic efficiency of a power station the former should be minimised and the latter maximised. A high ΔT tends to reduce the ΔP by reducing m (note the dependence on m^2) but this is somewhat offset by the increase of $\bar{T}$. The limit on achieving a low coolant inlet temperature is dictated by the economics of the helium/steam heat exchangers and the limit on ΔT is dictated by the stress limits of the structural materials of the blanket cells at high temperature and under bombardment by high energy neutrons.

Considering now the effect of operating pressure it can be seen from equation (1) that this should be maximised to reduce ΔP which, neglecting effects of changes in Ψ through viscosity changes, is linearly dependent on P. The pumping power fraction (which should be only a small fraction of total output) is given by:

$$K = \frac{\Delta P}{\bar{\rho}\, C_p \Delta T} \qquad (2)$$

Helium is a nearly perfect gas under most practical reactor operating conditions hence the mean density is directly proportional to the pressure. Thus, combining equations (1) and (2) shows that K decreases inversely proportionally to the square of the pressure level; hence it is highly important to maximise P.

The coolant operating pressure will be determined by the mechanical properties of the duct material and the prevailing standards of compressor design. The mechanical properties of the material will be affected by the surrounding environment i.e. by the synergistic and time dependent effects of working stress, heat and neutron fluxes and mean temperature during the working life of the material. The volume fraction of structure - or thickness of coolant pipes - must be limited to permit adequate breeding in the blanket. Although some small prototype reactors operate at up to 80 bar the limit for commercial compressor operation is currently between 50 and 60 bar. The effects and interactions of these limits on blanket cell design can be analysed quantitatively as follows.

It is first necessary to define some ranges of values for various blanket cell parameters. The following values are taken from the work of Mitchell and Booth (4).

Structure fraction (η)	= 0.02 - 0.06
Mean volumetric heating rate/ wall loading (α)	= $1.35 m^{-1}$
Cell minimum length ($L_c = 1/\alpha$)	= 0.75m
Axial length of coolant ducts (L)	= 5.0m
Inside diameter of coolant ducts (d_i)	= 10-30mm
Front wall area of cells (A_W)	= $0.28 m^2$

It can easily be shown that the wall thickness of the cell coolant ducts is given by:

$$t = \tfrac{1}{2}\sqrt{\frac{4\eta A_W L_c}{\pi n L} + d_i^2} - \frac{d_i}{2} \qquad (3)$$

Using the values set out in the previous paragraph the thicknesses have been calculated for a range of internal diameters and structure fractions, (Figure 4). This shows that for $\eta = 0.04$ and d_i

in the range 10-30mm the thickness may be in the range 5-50% of the inside diameter. The larger values of t would give rise to problems in manufacturing the tubes into spirals.

The heat generated in the lithium must be transferred to the helium through the walls of the cooling ducts. It can easily be shown (for example Kay, (7)), that for heat transfer through the wall of a straight pipe the temperature difference is given by:

$$\Delta\theta_{wall} = \frac{Q \log_e d_o/d_i}{2\pi k_t} \qquad (4)$$

and, ignoring any effects which might be due to the fact that the pipes are helical, we can apply this to the blanket cells.

A large area of uncertainty in the design of commercial fusion reactor blankets is the choice of materials of construction. The allowable stresses of many metals and alloys are known to decrease not only with temperature but also with neutron bombardment (some alloys, i.e. annealed stainless steels, may become stronger (Badger, (8)) but the evidence is not conclusive). A survey of creep of irradiated metals in fast reactors was carried out by Harries (9). The possibility of using ceramic/metallic alloys has been mooted but considerable development work would be required before they could be proposed with confidence. Among the many metallic alloys which have been proposed are stainless steel 316, TZM (basically molybdenum) and Inconel. Figure 5 shows the maximum allowable stresses (for unirradiated samples) of these materials (5) together with their thermal conductivities (10). The temperature difference across the blanket coolant ducts has been calculated for these three materials using equation (5), obtained by substitution from (3) into (4), and values are given in Figure 6.

$$\Delta\theta_{wall} = \frac{P_W A_W}{4nL\pi k_t} \log_e \left[\frac{4L_c nA_W}{\pi d_i^{\,2} nL} + 1 \right] \qquad (5)$$

Since the thermal conductivity data for Inconel are a tentative extrapolation from a few disparate data the values of $\Delta\theta_{wall}$ for Inconel and Molybdenum (TZM) are shown on the same curve evaluated with a k_t value (90 W m^{-1} $^oC^{-1}$) taken as a mean from Figure 6. The thermal conductivity used for stainless steel is 24 W m^{-1} $^oC^{-1}$ (valid at about 600°C). Figure 6 shows the effect of varying wall loading at a constant structure fraction of 0.04 and Figure 7 shows the effect of varying η at a wall loading of 4MW m^{-2}. It can be seen that the low k_t of stainless steel can give rise to large values of $\Delta\theta_{wall}$.

The hottest location in the duct will be on the lithium side at the outlet, where the temperature will be given by:

$$T = T_{out} + \Delta\theta_{film} + \Delta\theta_{wall} \qquad (6)$$

Hence, taking typical values of T_{out} and $\Delta\theta_{film}$, 600°C and 30°C respectively (see section 3), the maximum metal temperature in the coolant ducting can be calculated using the information in Figures 6 and 7. The appropriate maximum allowable stress can then be found from Figure 5 and the maximum operating pressure (from a material strength viewpoint) can be calculated from the Lamé equation:

$$P = f\left[\frac{d_o^{\,2} - d_i^{\,2}}{d_o^{\,2} + d_i^{\,2}}\right] \qquad (7)$$

The results are shown in Figure 8, for TZM and Inconel 718 and in Figure 9 for stainless steel. The reason for the complex shape of the curves especially for Inconel, $\eta = 0.04$, is that the maximum operating pressure is subject to conflicting effects as d_i changes. For constant η, as d_i increases the ratio $(d_o^2 - d_i^2)/d_o^2 + d_i^2)$ decreases but simultaneously, for constant P_W, the temperature drop through the tube wall decreases, Figure 7: consequently the maximum shear stress f increases. In most cases the decrease in the diameter ratio term outweighs the increase in f, hence P_W decreases as d_i increases. In other cases depending on the f - T characteristics of the material, the increase in f predominates.

The results show that advantage could be taken of the high maximum allowable stress of TZM and Inconel through a reduction in structure fraction. Figure 8 shows the effect of halving η for TZM; the curves are almost independent of P_W because of the small dependence of f on T in the region of interest. Figure 9 shows that for high wall loadings with stainless steel a structure fraction of 0.04 is approximately in line with the current compressor design limit. At low wall loadings and low values of d_i there is scope to reduce the structure fraction. For high d_i and high P_W the operating pressure may be limited by the stress consideration unless an increase in η is considered.

In these calculations it is assumed that the tube coil helix angle is varied to make the heat flux constant along the cooling tube length. Since the heat generation rate is approximately four times greater at the front of the cell than at the rear, the helix angle will be least at the front. Neglecting possible effects of the similar radiation gradient from front to rear of the cell it has been shown that it is possible (especially for stainless steel) that the working pressure is controlled by the material stress limit at the hottest point in the duct - i.e. the lithium side of the hot gas outlet. In this case the helix angle could be decreased at the rear, to decrease the local heat flux, $\Delta\theta_{wall}$, and hence the maximum wall temperature itself. If radiation effects were included the limit stress point could be much nearer the front of the cell.

3. BLANKET CELL ROWS

3.1 Introduction

The number of blanket cells in a row can be varied: here we consider 3, 4 or 5 as in the CCTR-II. As suggested by Figures 3 and 10a, the inlet and outlet manifolds will run one above the other along the back of the row of cells. Figure 10b shows that a number of manifold configurations are possible. The designer must consider whether the inlet and outlet are to be near to the same end (as in A-A) or far apart in the row (as in B-B.). Furthermore he must decide whether the supply and collector pipes will be opposite a blanket cell (as at A) or in the inter-cell position (as at C).

The design of blanket cell row ducting involves a number of criteria which may conflict. These criteria are (a) that the

pressure drop should be minimised, (b) that the coolant should be evenly distributed between the individual cells, and (c) that the weight should be minimised i.e. that the duct sizes be small. Since the flow will adjust such that the pressure drop through all the possible routes is identical, the maldistribution will be reduced if the pressure drop in the interconnecting ductwork is considerably less than in the blanket cells. This argument also suggests that an arrangement such as A-A in Figure 10b would display a large degree of maldistribution; for a given flowrate the path through cell 1 then presents a lower ΔP than that through cell 3 (due to the extra fittings and extra pipe length) and the coolant flows would adjust to starve cell 3. It can similarly be deduced that situating the supply pipe as shown is preferable to locating it at A.

The arrangement shown in Figure 10a, and with solid lines in Figure 10b, is that with the least maldistribution. Most of the calculations described here were carried out using that pattern to investigate the effects of interconnecting duct sizes on the pressure drop characteristics of the blanket cell row and to choose suitable values to carry forward to the torus segment calculations. A few calculations were carried out to examine the quantitative effects of changing the ducting pattern.

The characteristics of the cell rows were investigated by considering their constituent parts (blanket cells, straight pipes, dividing T's, joining T's and bends) writing the pressure drop and flow conservation equations for each and solving the resulting set of non-linear simultaneous equations. Appendix 1 presents the governing equations for all the units involved, together with a comment on accuracy. Appendix 2 describes the solution techniques developed for this problem. The results from the computer program give the mass flow and pressure at all the nodes in the blanket cell row.

3.2 Results for five-cell rows

The results of an initial set of runs are shown in Table 1:

In these calculations the following standard set of conditions were assumed:

Coolant inlet temperature	= 300°C
Coolant outlet temperature	= 630°C
Cell internal ducting diameter	= 20mm
Structure fraction	= 0.04
Wall loading	= 4.7 MW m^{-2}

The layout of the ducts is shown in Figure 12.

Table 1 gives the following information:

(i) Ducting diameter, D_s and D_r, on the supply and return sides respectively: D_s and D_r are uniform and not necessarily equal.

(ii) Total pressure drop, ΔP: This is taken from the point in the supply line just upstream of the inlet manifold to the point in the return line just downstream of the outlet manifold (see Figure 10a).

(iii) Pumping power fraction, K: The proportion of the total energy removal used in supplying the pressure drop in the blanket cell row, given by equation (2).

(iv) Maldistribution,

$$M = \left[\Sigma \left(\frac{W}{W_p} - 1\right)^2 \times \frac{1}{n_c}\right]^{\frac{1}{2}} \qquad (8)$$

M is zero if the flow of coolant is evenly distributed between the cells in a row, and M = 0.3 if, in a five cell row, the ratios of actual/desired flow for the cells are 1.25, 0.75, 0.5, 0.75 and 1.25. In this latter case the central cells would be starved and the outer pair overcooled.

(v) Maximum velocity, u_{max}: This is the maximum gas velocity at any point in the unit and is the greater of the velocities in the supply and return ducts. It is commonly suggested that the need to minimise erosion will limit the velocity to 60 ms^{-1}.

(vi) Mean gas temperature rise, ΔT and film temperature drop $\Delta\theta_{film}$: Due to the maldistribution some of the cells will be starved of coolant and will consequently experience larger values of ΔT and $\Delta\theta_{film}$ than the mean. Conversely some will experience lower values. The table gives the greatest and the least values of ΔT and $\Delta\theta_{film}$ for individual cells in the row.

(vii) Maximum inside wall temperature, $T_{i,max}$: The maximum coolant duct inside the wall temperature is given by:

$$T_{i,max} = T_{in} + \Delta T_{max} + \Delta\theta_{film,\ max} \qquad (9)$$

The pressure drop and pumping power fraction in a single blanket cell are 0.74 bar and 0.011 bar compared with the best figures in Table 1 of 0.8 and 0.012. In this case the duct inner wall temperature is 660°C (max) and with $\Delta\theta_{wall}$ = 60°C (Figure 7) the maximum temperature of the duct wall is 720°C. For stainless steel the corresponding maximum allowable stress is 24 MPa (Figure 6) and the maximum operating pressure 59.8 bar, which conveniently is at the compressor design limit. The use of TZM or Inconel with such operating parameters would, as discussed earlier, introduce the possibility of reducing the structure fraction.

The results in Table 1 are plotted in Figure 11 showing the effect on ΔP and K of varying D_s at fixed D_r and of varying D_r at fixed D_s. The maximum D_r and D_s are fixed by space considerations; to a first order $(D_s + D_r)$ < cell diameter or cell major dimension, allowing for duct wall thickness, lagging and space for lithium supply and return ducts. In this case with A = 0.28 m^2 the cell size is approximately 0.53 metres square and with duct diameters 0.25m we are near, but not above, the limit. The results illustrate that as D_s and D_r increase and the pressure losses in the ducting diminish so the overall ΔP and K are asymptotic to the value for a single cell, whilst simultaneously the maldistribution decreases (see section 3.1). Mitchell and Booth (4) suggested that for a complete coolant circuit K (referred to reactor thermal output) might be of the order of 0.02 and for the individual cells 0.012 (in the present case it is 0.011). It is suggested here that to

achieve the required overall K the value for a row of cells should be 1.2 x K for a single cell. Figure 11 suggests that this can be achieved with $D_s > 0.12m$, $D_r > 0.17m$. The respective coolant velocities in the ducts are then 67 and 52 m s^{-1}, hence to meet the velocity limit of 60 m s^{-1} D_s could be increased to 0.13m.

Table 1 shows that the maldistribution increases (a) as the duct diameters decrease and (b) as the difference in duct diameters increases (see section 3.1). It also shows, however, that at the possible minimum diameters, given above, the degree of maldistribution appears acceptable in that excessive metal temperatures are not encountered. Figure 11 shows that for acceptable D_s and D_r the overall pressure drop is more dependent on the return than on the supply duct sizes. The reason for this is that the pressure losses on the return side are significantly greater than on the supply side as shown in Figure 12 which presents the full results of the calculations for the case $D_s = D_r = 0.2m$. It can be seen that the pressure losses, reversible and irreversible, in the joining T's are larger than those in the dividing T's, especially in the final junction feeding the return pipe. In the case in Figure 12 the pressure loss here is 5.6% of the total, a figure which increases as the ducting diameters decrease, for $D_s = D_r = 0.075$ it is 59.9%. Figure 12 also shows that:-

(i) For the flows which continue straight-on at the diving T's, the pressure increase due to the decrease in velocity outweighs the irreversible pressure loss.

(ii) The pressure losses in the straight pipes are always negligible compared with the remaining pressure losses.

(iii) The pressure losses in the straight pipes and bends on the return side are greater than those in the equivalent units, with identical flowrates, on the supply side due to the change in density through the increase in temperature.

The correlation for pressure drop in dividing and joining flow used in this work was proposed by Vazsonyi (11) based on a variety of data by earlier workers. Other methods have been published by Idel'chik (12) and ESDU (13, 14). For the conditions of this work the various methods give results which agree to within about 25% for the preferred D_s and D_r although (i) they are based on experiments with water at lower velocities than those considered here, (ii) there is disagreement between ESDU and the other methods for D_s and $D_r < 0.05m$.

Data given by Idel'chik (12) show that the use of rounded junctions, Figure 13, can considerably reduce irreversible pressure loss. Calculations show that the irreversible loss could be reduced by an order of magnitude, however a penalty would be incurred since the bend radius would have to be approximately 2D and space limitations may not permit this.

We now examine the effects of changing some of the parameters used in the initial set of runs, and Table 2 shows some results for various values of d_i. If d_i is decreased, strength of materials considerations will allow an increase in pressure. Two conditions can be contemplated. Firstly one where advances in compressor design can allow advantage to be taken of the increase in pressure, and secondly one where we are obliged to keep the pressure at 59.8 bar, applicable to d_i = 20mm. The Table shows that a reduction in d_i, irrespective of whether advantage can be taken of the possible increase in pressure, causes K to be too large and indicates that 0.02m appears to be the likely minimum value for d_i, unless more than eight coolant tubes were used in each cell. For flow in a tube the pressure loss is proportional to $W^{1.75}/d^{4.75}$. Through the high dependency on d the 25% decrease in d_i has caused a fourfold increase in ΔP (sets C and B). Hence the pressure loss in the cells dominates the total and explains the small effect of D_s and D_r. The dependency of ΔP on $W^{1.75}$ shows that the number of tubes per cell has to be increased to 16 if d_i is reduced from 0.02m to 0.15m and the pressure drop is not to change.

For an increase in d_i to 0.025m it is also possible to envisage two possible pressures (sets D and E). The use of stainless steel limits the pressure to 42 bar in which case the pressure drop is approximately halved compared with the standard case, set C; the K values are reduced by about 30%. Alternatively the pressure may be limited by the compressor design limit, set E, in which case ΔP and K are further reduced.

An increase of d_i is accompanied by a decrease of $\Delta\theta_{film}$. For d_i = 0.015, 0.020 and 0.025m, the temperature differences are respectively 38, 30 and 25 degrees C.

Another important parameter is the flow-rate of coolant to the cells, $P_W A_W/C_p \Delta T$; so far 0.77 kg s^{-1} for the standard conditions Figure 14 shows the effect of varying the coolant flowrate as well as of varying d_i and $\bar{T}$. D_s and D_r were taken as 0.2m, A as 0.28m^2 and the pressure as 60 bar. The mean temperature level is seen to have little effect while d_i has a significant effect on the overall pressure drop.

Finally in connection with five-cell rows, the effect of piping layout symmetry is investigated using the three arrangements shown in Figure 15, and the results are given in Table 3 for the standard operating parameters.

Table 3 shows that increasing the asymmetry reduces the pressure drop at small D but has negligible effect at large D; it also increases the maldistribution at all D. However in the size range of D_s and D_r shown earlier to give acceptably low values of P and K, M is generally satisfactory showing that the layout may not be an important parameter.

3.3 Three-cell rows

It now remains to examine whether the number of cells in a row is an important parameter in determining performance. The CCTR-II-A design incorporates 3, 4 and 5 cell-rows, and we examine the 3-cell row,

which differs most from the five-cell row considered in section 3.2. Table 4 shows the results of calculations on the layout shown in Figure 16 - again using the standard conditions.

For a given size and rating the total flow is only 60% of that in a five-cell row. Since the pressure drop in the blanket cells is unchanged the contribution in the joining ducting is reduced. Hence the overall pressure drop and maldistribution decrease with the number of cells in the row.

An opposite conclusion would be reached if we considered a cell-row of constant total first wall area with given wall loading and rating. Here the total flow per cell would be increased and the pressure drop and maldistribution would increase (for given d_i).

3.4 Conclusions

The work presented in this section has shown that it is possible to design the ducting for blanket cell rows such that, within the space limitations discussed in section 3.2, the pressure drop is not excessively greater than that in the individual blanket cells, i.e. not more than 20% greater. When the pressure drop is at such an acceptable value, neither maldistribution of coolant flows nor the layout of the coolant ducting between the blanket cells are limitations on the design.

It has been shown that for CCTR-II-A the coolant ducting diameter within the cells should be not less than 20mm. In the configurations examined, the performance of the row of blanket cells is more sensitive to the size of the outlet ducting and thus D_r should be greater than D_s.

4. HALF SEGMENTS AND COMPLETE COOLING CIRCUITS

This section considers the ducting which joins the blanket cell rows into half segments and finally the complete cooling circuits which include pairs of half segments, compressors and steam raisers.

We begin by considering the primary pipes in a half segment, i.e. the supply and return pipes which carry the entire coolant flowrate. Space considerations dictage (see Figure 1) that the two pipes side-by-side, together with lagging and a gap (G) to allow room for remove cutting and welding should occupy a width no more than the outer width of the half segment.

The width of the half segment in CCTR-II, at its outermost point, is 2.65m, hence

$$2D'_i + 4t_L + 4t_{SF} + G = 2.65 \qquad (10)$$

In CCTR-II the blanket and ducting are within the primary vacuum and the function of the lagging is to minimise heat loss by radiation. This requires a considerably lower thickness than the reduction of conduction heat loss. Allowing 50mm as a reasonable estimate for t_L and 0.2m for G equation (10) becomes

$$D'_i + 2t_{SF} = 1.12 = D'_o \qquad (11)$$

Hence equation (7) can be rewritten in the form

$$D'_i = 1.12\left(\frac{1 - P/f}{1 + P/f}\right)^{\frac{1}{2}} \qquad (12)$$

An outlet gas temperature of 630°C was again assumed and the appropriate allowable stresses found from Figure 5. Equation (12) as then solved using these stresses to give the maximum allowable external diameter of the main coolant duct as a function of the operating pressure (Figure 17). As a minor correction to this calculation it should be noted that the allowable stresses on the inlet, low temperature, side are higher than on the outlet and the inlet duct maximum diameter could be correspondingly increased.

The coolant velocity limit (60 m s^{-1}) imposes a minimum constrant on D'_i depending on the pressure and on the mass flowrate of the coolant ($n_s P_W A_W / C_p \Delta T$). Figure 17 shows this minimum diameter for the conditions of CCTR-II-B (n_s = 62, P_W = 4.7MW m^{-2}) assuming ΔT to be 330°C. The effect of changing coolant flowrate, and hence P_W, but keeping ΔT constant is also shown. Adding the compressor design operating limit (60 bar) to Figure 17 shows a closed operating envelope for three coolant flowrate/metal combinations; that for P_W = 4.7MW m^{-2}, coolant mass flow 47.5kg s^{-1} and stainless steel being shaded. Based on this analysis the maximum possible wall loadings in CCTR-II-B are, for stainless steel 14.9MW m^{-2} and, for TZM/Inconel, 17.0MW m^{-2}. Each envelope also suggests a minimum operating pressure which arises through the fact that, in order to maintain the velocity below the maximum, decrease in pressure (and hence in density) must be accompanied by an increase in D'_i. However, D'_i is limited through space and stress considerations (mainly the former) and thus determines the minimum operating pressure.

We now examine in detail the coolant flow in a half segment, to ascertain the likely pressure drops and maldistribution, in an analysis similar to that given for cell rows in section 3. Figure 18 shows a simplified diagram of the supply ducting of the CCTR-II-A; the return ducting could be interposed upon it. The standard conditions defined earlier were assumed and the primary return duct diameter was fixed to give a coolant velocity of 50 m s^{-1}, operating at point A in Figure 17. A velocity somewhat less than the maximum, 60 m s^{-1}, was chosen in order to allow some increase of wall loading without immediately violating the constraint. For simplicity the supply duct sizes were chosen to equal those on the return side in which case the velocity is 31m s^{-1}, although there is clearly scope to reduce the supply duct size. The remaining duct diameters in the inter-row piping were calculated assuming that each cell row receives its correct proportion of the coolant flow and that the above velocities are maintained.

The lengths of the tubes in the segment ducts are given in Figure 2 and, as shown in Figure 18, all the pipe junctions are assumed to be at right angles. This is therefore a pessimistic model and pressure drop and distributions will be worst-case results. In practice, radius bends will be used where space permits in a final ducting system.

The duct diameters in Figure 18 show that the values of D_s and D_r for the three, four and five cell rows are 0.13, 0.16 and 0.18m. These sizes were shown earlier to give reasonable pressure drop, < 20% more than for a single cell, and reasonably low M.

The overall pressure loss in the half-segment model (Figure 18) is 1.01 bar of which 0.79 bar occurs in the cell-rows (0.74 bar in the individual cells) and the remainder in the main ducting. Figure 19 gives the ratios of actual to required flows to the blanket cell rows - indicating good distribution and the remaining variations can be corrected by refinements in duct design or perhaps by gagging. It is also worth noting that constant wall loading around the minor circumference of the torus has been assumed; this will not be the case in practice and minor adjustments to individual cell and row coolant feed rate will be necessary.

It remains to analyse the half segment as part of a complete reactor cooling circuit, comprising two half segments with a common steam raiser and compressor. It is necessary to make some assumptions about the helium pressure losses external to the reactor. Following Idel'chik (12), and assuming that the primary feed ducts and returns for the two half segments will, in each case, be joined in an arrangement similar to Figure 13, i.e. neglecting possible space limitations external to the reactor, the pressure loss in the primary join and divide are calculated to be small, about 2×10^{-3} bar. Assuming straight pipe runs of 50m between the segment, compressor, boiler and back to the segment, and coolant velocities of 50m s^{-1} indicates a contribution of 4×10^{-3} bar to the total pressure loss. Modern steam raiser design suggests a pressure loss of the order of 0.3 bar in the boilers. Thus taking into account also control valves and bends, a reasonable estimate of the total pressure loss in the circuit external to the half segments might be 0.35 bar. Hence for the present case the overall pressure loss is 1 + 0.35 = 1.35 bar, and the corresponding pumping power fraction given by

$$K = \frac{\Delta P}{\bar{\rho} C_p \Delta T \eta_c} = 0.021 \qquad (13)$$

in which a compressor efficiency of 0.95 is assumed.

Having examined one possible scheme it remains to consider the effect of changing operating and design parameters. The first is the diameter of the segment ducting. A set of runs was carried out with all the diameters in Figure 18 multiplied by some constant factor, all the operating parameters maintained as in the standard conditions. Figure 20 shows the results which illustrate that any significant reduction in duct sizes, apart from leading to excessive coolant velocities, greatly increases the pumping power fraction and maldistribution.

A final series of runs was carried out in order to investigate the effect of wall loading and coolant temperature rise, using the duct sizes shown in Figure 19, the standard conditions and a pressure of 60 bar. Figure 21 shows a plot of the results. For each ΔT it shows the corresponding thermodynamic efficiency, defined for the helium side by

$$\eta_{th} = \frac{\Delta T}{T_{out}} \qquad (14)$$

It is now possible to draw a design option region for the possible conditions in the reactor. The limits of operation are fixed by the maximum metal temperature, maximum pumping power fraction, economic target wall loading and minimum thermodynamic efficiency. Most of these limits are not, however, independent: for example, if the thermodynamic efficiency of the reactor design chosen were high there would be scope for allowing an increase in pumping power fraction - leading to a decrease in weight and cost through a decrease in duct sizes. Again an economic wall loading limit will be based on reactor costs and will depend on construction materials. In order to illustrate the design option region we consider here certain fixed limits:-

$$K < 0.025$$

$$\eta_{th} > 0.36$$

$$P_w > 4 \text{MW m}^{-2}$$

These limits are shown, for example, in Figure 22a, where the light and dark lines represent 40 and 60 bar operating pressures. The fourth constraint, maximum metal temperature depends on the material and is evaluated as in the following arguments for Inconel at 60 bar.

Using the standard operating conditions, applicable to Figure 22a, i.e. $\eta = 0.04$, d_i = 20mm, we find from Figures 4 and 5 and Equation (7) that the maximum temperature in the cell coolant ducts is 740°C, see Figure 22a. Now the maximum value of $\Delta\theta_{wall}$ is about 25°C and $\Delta\theta_{film}$ with low K is about 30°C (Table 1). Hence the maximum bulk gas outlet temperature is 740 - 30 - 25 = 685°C and, for T_{in} = 300°C, this indicates the maximum ΔT of 385°C.

The shaded region in Figure 22a indicates the design option region within which all the constraints which we have imposed are satisfied. The region suggests a maximum wall loading where $P_w A_w / C_p \Delta T$ is 0.96 kg s^{-1} and $T_{t,max}$ is 740°C, ΔT = 385°C. Hence the maximum wall loading is 6.9MW m^{-2}.

If the pressure is reduced to 40 bar (light lines in Figure 22a) an increase in operating temperatures is permissible owing to the lower imposed stresses but K is increased (for given flow per cell) due to the decreased density and increased ΔP (see section 2). In the case of Inconel there appears then to be no region within which all the imposed constraints are satisfied. For these conditions it would be necessary to change a constraint e.g. increase K to say 0.035, reduce P_w to ~ 3.5 MW m^{-2} or increase the metal temperature.

Figures 22b and 22c give the same information for TZM and stainless steel respectively. In the former case the maximum wall loadings, for 40 and 60 bar, are 6.6 and 10.6MW m^{-2}. Thus TZM, which would entail a high capital, and development, cost would permit an advantageous increase in permissible wall loading. For stainless steel, however, Figure 22c suggests that no design option region is possible within the above constraints and that it would be necessary to relax two of the constraints to produce such a region.

Design option regions are illustrated for other sets of conditions in Figure 23. The thick curves show conditions similar to the corresponding curves in Figure 22 except that the inlet temperature is reduced to 200°C. This has the effect of an increase in ΔT within the maximum metal temperature constraints as well as of a small decrease in ΔP (see Figure 14). Figures 23 a-c show that the design option regions are considerably expanded. The maximum P_w for Inconel, TZM and stainless steel are respectively 11.5, 12.5 and 8.8 MW m^{-2} which should be compared with the values for T_{in} = 300°C (6.8, 10.6 and 4.9 MW m^{-2}) showing the potential

advantage in reducing T_{in} and increasing ΔT.

Finally we examine (light lines in Figure 23) the effect of a decrease in pressure to 40 bar accompanied by an increase in d_i to 25mm while maintaining the standard T_{in}, 300°C. This set of examples is then directly comparable with those shown in the light lines in Figure 22 differing only in d_i. The resultant decrease in ΔP in the blanket cells is accompanied by a significant reduction in the overall pumping power fraction; the constraints can now be satisfied for all the candidate materials considered here. Since the flow resistance of the blanket cells is lower than that in the comparable case in Figure 22 but the reisistance of the interconnecting ductwork is unchanged, the maldistribution is increased, from 0.029 to 0.068. While not excessive, this might require an increase in segment duct sizes with a consequent increase in weight.

In the foregoing paragraphs we have examined the construction of design option regions within specified independent constraints. In practice, as we have seen, these constraints will not be independent, and the boundaries of the regions will be modified accordingly. The design point, located in this region, will be finally selected when (a) cost and cost sensitivity data are refined, (b) further technical data (pressure drop, materials properties and blanket cell heat load distribution) are available, and (c) all the constraints and their interdependence will have been determined.

It has been suggested (6) that space requirements may become crucial for fitting pipes and bends in the available space for the ducting within the cell rows and that joining the cell rows. This study has been limited to the geometry of the CCTR-II-A design and to right angled bends; radius bends with larger space requirements but smaller ΔP would give somewhat different design option regions. It should also be noted that maximum stress levels used here originate from tests on unirradiated samples at constant strain. Due to the radiation environment and to the cyclic operation of a reactor these conditions will not hold and the maximum P_w may be reduced. The consequent reduced gas flows may ease the space constraint by reducing the duct sizes.

5. CONCLUSIONS

Based on a hierchical study of the coolant flow in the ducting network of a gas cooled fusion reactor, it has been shown that it is possible to draw design option regions satisfying certain defined criteria. The regions depend on the temperature and pressure of the coolant, the ducting geometry and the construction material.

The mathematical techniques evolved in this study can be used for any network system for which the pressure drop characteristics of the individual units are known and it is to be expected that further use will include such items as junctions not leaving at right angles and curved pipes.

As an alternative to the separate supply and return duct arrangement, it has been suggested that a concentric system might be adopted whereby the hot gas from the reactor flows in pipes within those carrying the cool gas supply. Such a system, which has already been advocated for HTR operation (15), reduces the stress in the hot pipe, one of the limiting constraints due to the implied maximum temperature. The inner, hot, pipe is made of fittings identical to those considered in this study. However, the outer, cool gas flows in the annulus and the flow at the junctions will be complex, for example the flow continuing straight at one side of a dividing T will flow round the side branch of the inner pipe. The behaviour of such junctions is unknown though it is believed that they will show increased pressure drop and pumping power requirements - an experimental study of such junctions is in hand to provide the necessary correlations.

6. ACKNOWLEDGEMENTS

Thanks are due to J T D Mitchell and R G Owen (Harwell) for useful discussions in the course of this study. Thanks are also due to I P Jones (Harwell) for work on the mathematical techniques of network analysis and also for writing the Appendix 2.

7. REFERENCES

(1) Hunt, J C R and Hancox, R. The use of liquid lithium as coolant in a toroidal fusion reactor, Culham Report No. R-115, 1971.

(2) Lyall, H G. A comparison of helium and CO_2 as reactor coolant, Journal of Nuclear Energy 26, 49-60, 1972.

(3) Conn, R W and Kuo, S C. An advanced conceptual Tokamak Fusion Power Reactor utilising closed cycle helium gas turbines. Nuclear Engineering and Design 39, (1), 45-72, 1976.

(4) Mitchell, J T D and Booth, J A. Wall loading limitations in a helium cooled fusion reactor blanket, Culham Report No. R-126, 1973.

(5) Anon. Conceptual design study of a non-circular Tokamak Demonstration Fusion Power Reactor. Gulf Atomic San Diego Report No. GA-Ak3992, 1976.

(6) Mitchell, J T D, and Hollis, A. A Tokamak Reactor with servicing capability. Proceedings 9th SOFT Conference, Garmisch-Partenkirchen 1976, p 429.

(7) Kay, W M. An introduction to fluid mechanics and heat transfer. Cambridge University Press, London, 1963.

(8) Badger, B. UWMAK-III, a high performance non-circular Tokamak power reactor design. Fusion Feasibility Study Group, Nuclear Engineering Department Report UWFDM-150, University of Wisconsin, 1975.

(9) Harries, D R. Irradiation Creep in non-fissile metals and alloys. Journal of Nuclear Materials 65, 157-173, 1977.

(10) Perry, R H and Chilton, C H. Chemical Engineers Handbook. McGraw Hill Book Co. N.Y. Fifth Edition, 1973.

(11) Vazsonyi, A. Pressure losses in elbows and duct branches. Trans ASME 66, 177-183, 1944.

(12) Idel'chik. Handbook of hydraulic resistances USAEC Report No. AEC-TR-6630, 1966.

(13) ESDU. Pressure losses in three leg pipe junctions: Dividing flows. ESDU item No. 73022, 1973.

(14) ESDU. Pressure losses in three leg pipe junctions: Combining flows. ESDU Item No. 73023, 1973.

(15) Fortescue, P, Nicholl, D, Rickard, C and Rose, D. HTGR - underlying principles. Nucleonics, 18, (1), 86-90, 1960.

(16) Ruffell, A E. The application of heat transfer and pressure drop data to the design of helical coil once-through boilers. Symposium on multi-phase flow systems. University of Strathclyde Paper I5, 1974.

(17) Reid, J K. Fortran Subroutines for the solution of sparse systems of non-linear equations, AERE Report No. R-7293, 1972.

NOMENCLATURE

A_W	Front wall area of a cell	m^2
C_P	Specific heat capacity	$J\ kg^{-1}\ ^oC^{-1}$
d	Diameter of blanket cell coolant ducts	m
D	Diameter of inter-cell manifold ducting	m
D'	Diameter of inter-row ducting	m
D_{coil}	Diameter of cell coolant duct coil	m
G	Gap between main coolant pipes	m
k_t	Thermal conductivity of cell coolant ducts	$W\ m^{-1}\ ^oC^{-1}$
K	Pumping power fraction of reactor thermal output	-
l	Length of straight pipe	-
L	Length of coolant tubes within cells	m
L_C	Length of blanket cells	m
m	Flowrate in each cell coolant duct	$kg\ s^{-1}$
M	Maldistribution	-
n	Number of coolant tubes per cell	-
n_c	Number of cells per row	-
n_s	Number of cells per segment	-
P	Pressure	Nm^{-2}
Q	Heat flow per unit length of tube	Wm^{-1}
R	Gas constant for helium	$J\ K^{-1}$
t	Wall thickness of cell coolant tubes	m
t_L	Lagging thickness	m
t_{SF}	Wall thickness of main coolant feeder tube	m
T_i	Temperature of inner surface of ducts	^oC
T_{in}	Coolant inlet temperature	^oC
$T_{t,\ max}$	Maximum metal temperature	^oC
$\overline{T}$	Mean coolant temperature	^oC
ΔT	Coolant temperature increase	^oC
u	Velocity	$m\ s^{-1}$
u_{max}	Maximum velocity in a cell-duct row	$m\ s^{-1}$
W	mass flowrate	$kg\ s^{-1}$
W_P	Mass flowrate in a cell for zero maldistribution	$kg\ s^{-1}$
W_T	Total mass flowrate per row of blanket cells	$kg\ s^{-1}$
α	Mean value of volumetric rate of energy deposition in cell/wall loading	m^{-1}
η	Structure fraction	-
η_C	Compressor efficiency	-
η_{th}	Thermodynamic efficiency	-
$\Delta\theta_{film}$	Temperature difference across gas film	^oC
$\Delta\theta_{wall}$	Temperature difference across cell coolant duct	^oC
ρ	Density	$kg\ m^{-3}$
$\overline{\rho}$	Mean density	$kg\ m^{-3}$
Ψ	Friction factor	-

Subscripts

i	Inside
o	Outside
r	Return
s	Supply

APPENDIX 1

This Appendix presents the pressure drop and flow conservation equations for the various units into which the blanket cell row can be notionally divided. The numbering schemes are shown in Figure A1. The solution scheme for the complete set of non-linear simultaneous equations is described in Appendix 2.

(a) Blanket cells

The pressure loss equation (see also equation (1) in the main text) is

$$P_1 - P_2 = \frac{1}{2}\left[\left(\frac{4m}{\pi d_i^2}\right)\right]^2 \frac{\psi}{d_i} \frac{RL}{P} \bar{T} \qquad (A-1)$$

The friction factor is given by the equation

$$\psi = 0.015 + 2.53\left[\left(\frac{d_i}{d_{coil}}\right)\right]^{0.275} Re^{-0.4} \qquad (A-2)$$

derived by Ruffell (16) from experiments on commercially rough tubing. Equation (A-2) gives friction factors about 4 times higher than correlations for straight tubes, e.g. equation (A-5) under the conditions in CCTR-II-A.

The flow conservation for a blanket cell, as for all units with no branches, is simply given by

$$W_1 - W_2 = 0 \qquad (A-3)$$

(b) Straight pipes

The pressure loss equation is

$$P_1 - P_2 = \frac{1}{2}\psi\rho u^2 \frac{1}{D} \qquad (A-4)$$

The friction factor is given by

$$\psi = 0.079\ Re^{0.25} \qquad (A-5)$$

In most of the cases considered the friction pressure loss in the straight tubes is small compared with the other pressure losses in the cell rows.

(c) Dividing flow (Type 1)

Two pressure drop equations can be written

$$P_3 - P_1 = \frac{\rho}{1.6}(1.8u_1^2 - 0.368\ u_1\ u_3) \qquad (A-6)$$

$P_3 - P_1$ is the total frictional and accelerational pressure drop. This equation, and all those following for 90° bends and T's, is based on the work of Vazsonyi (11). A factor of 1.25 has been included to account for the effect of closely placed branches. Similar to equation (A-6) we can write

$$P_2 - P_3 = \frac{\rho}{1.6}(1.8u_2^2 - 0.368\ u_2u_3) \qquad (A-7)$$

This form of equation is also used for 90° bends.

The flow conservation equation for this unit is written

$$W_1 + W_2 - W_3 = 0 \qquad (A-8)$$

(d) Dividing flow (Type 2)

The pressure drop equations are

$$P_1 - P_3 = \frac{\rho}{1.6}(1.8u_3^2 - 0.368\ u_3u_1) \qquad (A-9)$$

$$P_1 - P_2 = (1.36u_2^2 - 0.64u_1^2 - 0.72\ u_1u_2) \qquad (A-10)$$

and the flow conservation equation is

$$W_1 - W_2 - W_3 = 0 \qquad (A-11)$$

(e) Joining flow (Type 1)

$$P_1 - P_3 = \frac{\rho}{1.6}\ x$$

$$\left[2u_3^2 - 0.4u_1^2 - 0.41\ u_3\left(u_1 \frac{W_1}{W_3} + u_2 \frac{W_2}{W_3}\right)\right] \qquad (A-12)$$

$$P_2 - P_3 = \frac{\rho}{1.6}\ x$$

$$\left[2u_3^2 - 0.4u_2^2 - 0.41\ u_3\ \left(u_2 \frac{W_2}{W_3} + u_1 \frac{W_1}{W_3}\right)\right] \qquad (A-13)$$

$$W_1 + W_2 - W_3 = 0 \qquad (A-14)$$

(f) Joining flow (Type 2)

The governing equations are

$$P_1 - P_2 = \frac{\rho}{1.6}\ x$$

$$\left[2u_2^2 - 0.05u_1^2 - 2u_2\ (0.205\ u_3 \frac{W_3}{W_2} + u_1 \frac{W_1}{W_2})\right] \qquad (A-15)$$

$$P_3 - P_3 = \frac{\rho}{1.6}\ x$$

$$\left[2u_2^2 - 0.4u_3^2 - 2u_2\ (0.205\ u_3 \frac{W_3}{W_2} + u_1 \frac{W_1}{W_2})\right] \qquad (A-16)$$

$$W_1 + W_3 - W_2 = 0 \qquad (A-17)$$

APPENDIX 2

The Numerical Solution of the Pipe Network Equations

by

I. P. Jones

1. INTRODUCTION

The method used to solve the equations describing a network of pipes can be conveniently divided into three parts:-

(a) the specification of the network to the computer program;

(b) the construction of the set of equations describing the flow within the network;

(c) the solution of these equations.

All these parts need to be made as easy to use as possible, ideally only needing a simple specification of a network, the rest of the solution procedure being carried out automatically. Furthermore, it should be straightforward to change the network, adding or removing components from the system with only small changes to the input data. Finally it should be easy to add new types of components to those already used.

The method described in this appendix has these advantages and potentially provided powerful tools for the solution of other network problems.

2. THE SPECIFICATION OF THE NETWORK

The method adopted here is to number uniquely the start and finish of each unit in the network in an arbitrary order, as in Figure A2.

Each of these numbered points will have two variables associated with it, representing the values of the flowrate and the pressure at that particular point. The aim of the solution procedure will be to find the values of those variables at the numbered points. Each node of the network may now be specified, again in an arbitrary order, as the type of component, e.g. dividing T, straight pipe, bend, inlet, etc., together with the numbered points, which intersect at that node. At the same time any physical parameters associated with the components, e.g. radii or lengths, may also be specified. For example, the intersection of the numbered points 2, 3 and 5 may be specified as a dividing T junction, with point 2 as the main stream, dividing to form streams 3 and 5. Similarly the section joining points 3 and 4 may be specified as a straight pipe joining these two locations. The length and the radius of this straight pipe may also be input at the same time. This information is read in by the program using a simple format.

Inside the program a table of integers is constructed from the input data. This table is essentially a two-dimensional array with each component of the system being represented by one column of the array. The first entry in each such column is an integer representing the type of component, e.g. (1) for an inlet, (2) for a straight pipe, etc. The rest of the elements in the columns are integer pointers to the relevant quantities needed in equations for that component, for example to lengths of sections of pipes in an array of pipe lengths. This table is all that is needed to specify completely the network internally. It may also be checked easily to ensure that the network is complete and that the information is self-consistent.

3. THE CONSTRUCTION OF THE NETWORK EQUATIONS

The non-linear equations governing the complete pipe network may be written in the vector form

$$\underline{F}\ (\underline{n}) = 0 \qquad \text{(B-1)}$$

where $\underline{n}$ is the vector of unknowns, the flow rates and the pressures. These equations are given in Appendix 1. The inlets and outlets are also incorporated into this scheme with simple equations for the pressures and velocities, e.g. $W - W_I = 0$, where W is the flow rate and W_I the inlet flow rate. This device permits considerable simplification of the computer programming and eliminates many special cases. The solution procedure adopted for the equations (B-1) only requires the vector of residuals,

$$\underline{r} = \underline{F}\ (\underline{x}) \qquad \text{(B-2)}$$

for any vector of unknowns $\underline{x}$ and then automatically chooses $\underline{x}$ to make the residuals $\underline{r}$ small. The remainder of this section will be devoted to a description of the calculation of these residuals from the table of integers mentioned in the previous section, and a vector of unknown.

The table is scanned, column by column, and the first entry in each column, the specification of the type of component, is used as the argument of a Fortran computer GO TO to jump to the relevant section of code for that type of component. The residuals for that particular component are calculated in that section, from the equation given in Appendix 1, using the remaining entries in the column to locate any required physical quantities. Provided that the self consistency checks have been carried out during the first stage of the calculation, it can be seen that for n different components this procedure automatically generates the $2n$ residuals for each of the $2n$ variables.

This implementation is very flexible and new types of components can be added very easily to the system by extending the range of the computed GO TO. This scheme is also independent of the ordering of the variables and the components and so altering the network does not involve large recoding exercises, only simple changes to the input data.

4. THE SOLUTION OF THE GOVERNING EQUATIONS

As discussed in the previous section it is a straightforward task to construct the residuals, $\underline{r} = \underline{F}\ (\underline{x})$, given the unknowns $\underline{x}$. This section deals with the numerical method used to choose $\underline{x}$ in order to make the residuals $\underline{r}$ 'small'.

For a typical network problem, the equations for any component involve only a few variables and are termed 'sparse'. For efficient computation of such problems, we use a modification of Newton's method such that the method converges to a solution even with a poor starting approximation. This method is contained in subroutine NS03A from the Harwell Subroutine Library, Reid (17). When using this solution procedure, the variables must be scaled so that they are similar in magnitude. Here this was done using non-dimensional flow - W/W_I and pressure drops - $(P-P_I)/P_I$. Solving the system for pressure drop, rather than pressure, has the further advantage of reducing numerical cancellation errors because $\Delta P << P$.

Whilst this method is designed to converge from a poor estimate of the solution, computer time is more reasonable if good estimates are used in the beginning and if the residuals are scaled to

be of equal importance. To obtain a good initial estimate of the solution, the procedure is carried out by weighting down the importance of the non-linear pressure drop equation. This solution is then used as the initial approximation for the procedure using a more realistic scaling of the residuals. For the first case the residuals are scaled by dividing the mass balance equations by the inlet flow rate W_I, and the pressure drop equations by the inlet pressure P_I.

The initial approximation for this case is obtained empirically by assuming that the pressures are close to their inlet values and the flowrates equal to the values given by symmetrical flow through the unit. They are taken as simple ratios (< 1) of the inlet flow which are given separately to the program. Since the inlet pressure is typically very large, this procedure emphasises the linear mass balance equations, and reduces the importance of the difficult non-linear pressure drop equations. As a result the entire system of equations is fairly easy to solve and a solution can then be obtained quite quickly.

The values of the unknown $\underline{x}$ obtained by this procedure are then used as the initial values for the solution procedure. On this occasion, however, the importance of the pressure drop equations is enhanced by now scaling pressure drop residuals, typically by $\frac{0.01\ P_I}{n}$, where n is the number of components in the system. This procedure has worked well in practice, taking about 2 seconds C.P.U. time on an IBM 370/168 computer for a problem with about 120 components, i.e. 240 variables. If this double solution procedure is not followed and an attempt made to solve the full equations directly with only a rough initial guess, the subroutine takes very many iterations reducing the residuals by only a very tiny fraction at each step.

TABLE 1

Calculated performance for a five-cell row

D_s/m	D_r/m	ΔP/bar	K	M	u_{max}/ms^{-1}	$\Delta T^{\circ}C$ max/min	$\Delta\theta_{film}$/°C max/min	T_i(max)/°C
0.05	0.05	18.1	0.268	0.113	602	$^{382}/_{283}$	$^{35.9}/_{21.3}$	718
0.075	0.05	16.9	0.250	0.235	602	$^{503}/_{249}$	$^{63.8}/_{17.6}$	867
0.10	0.05	16.8	0.247	0.290	602	$^{561}/_{241}$	$^{77.7}/_{16.8}$	939
0.05	0.075	5.01	0.074	0.161	382	$^{468}/_{285}$	$^{52.7}/_{22.3}$	821
0.075	0.075	4.01	0.059	0.059	267	$^{350}/_{305}$	$^{32.9}/_{25.5}$	714
0.10	0.075	3.85	0.057	0.086	267	$^{375}/_{297}$	$^{37.0}/_{24.4}$	713
0.05	0.10	2.97	0.044	0.186	382	$^{490}/_{272}$	$^{57.6}/_{20.4}$	848
0.075	0.10	1.95	0.029	0.047	151	$^{362}/_{316}$	$^{34.8}/_{27.3}$	697
0.10	0.10	1.79	0.026	0.027	151	$^{399}/_{319}$	$^{31.2}/_{27.8}$	670
0.20	0.10	1.72	0.025	0.040	151	$^{350}/_{315}$	$^{33.1}/_{27.3}$	683
0.05	0.20	2.05	0.030	0.199	382	$^{503}/_{267}$	$^{60.3}/_{19.6}$	863
0.10	0.20	0.91	0.013	0.021	96	$^{343}/_{322}$	$^{31.7}/_{28.4}$	675
0.20	0.20	0.84	0.012	0.002	38	$^{331}/_{329}$	$^{29.8}/_{29.6}$	661
0.075	0.25	1.03	0.015	0.062	267	$^{370}/_{306}$	$^{36.2}/_{25.9}$	706
0.20	0.25	0.81	0.012	0.001	24	$^{331}/_{330}$	$^{29.8}/_{29.6}$	661
0.25	0.25	0.80	0.012	0.001	24	$^{330}/_{330}$	$^{29.7}/_{29.6}$	660

TABLE 2

Calculated performance for a five-cell row: Effect of changing d_i

	d_i/m	D_s/m	D_r/m	ΔP/bar	K	P/bar	
	0.015	0.15	0.15	2.17	0.021	89.1	
A	0.015	0.20	0.20	2.08	0.021	89.1	Advantage taken of increase in allowable pressure
	0.015	0.25	0.25	2.05	0.020	89.1	
	0.015	0.15	0.15	3.24	0.047	59.8	
B	0.015	0.20	0.20	3.10	0.045	59.8	Pressure same as for d_i = 0.02m - set C
	0.015	0.25	0.25	3.06	0.045	59.8	
	0.02	0.15	0.15	0.97	0.015	59.8	
C	0.02	0.20	0.20	0.84	0.012	59.8	Compare set B
	0.02	0.25	0.25	0.80	0.012	59.8	
	0.025	0.15	0.15	0.66	0.014	42.0	
D	0.025	0.20	0.20	0.48	0.010	42.0	Sets A - D are for stainless steel ducts
	0.025	0.25	0.25	0.42	0.009	42.0	
	0.025	0.15	0.15	0.47	0.007	59.8	
E	0.025	0.20	0.20	0.34	0.005	59.8	Use of TZM or Inconel. P Limited by compressor
	0.025	0.25	0.25	0.30	0.005	59.8	

TABLE 3

Calculation of performance of a five-cell row: Effect of changing duct layout

D_s/m	D_r/m	ΔP/bar	K	M	T_i(max)/°C	
0.05	0.05	18.1	0.268	0.113	718	Original layout as in Figure 12
0.15	0.15	0.98	0.015	0.006	662	
0.20	0.20	0.84	0.013	0.002	661	
0.05	0.05	16.2	0.223	0.750	1176	Layout (i) in Figure 15
0.15	0.15	0.99	0.015	0.026	676	
0.20	0.20	0.84	0.013	0.007	664	
0.05	0.05	11.9	0.179	0.920	1258	Layout (ii) in Figure 15
0.15	0.15	0.99	0.015	0.037	670	
0.20	0.20	0.84	0.013	0.012	665	

TABLE 4

Calculation of performance of a three-cell row

D_s/m	D_r/m	ΔP/bar	K	M	$T_{i(max)}$/°C
0.05	0.05	7.22	0.105	0.147	738
0.10	0.10	1.17	0.017	0.020	667
0.25	0.10	1.12	0.017	0.021	669
0.20	0.20	0.80	0.012	0.001	661
0.10	0.25	0.83	0.012	0.012	665
0.25	0.25	0.79	0.012	0.001	660

TABLE 1

Calculated performance for a five-cell row

D_s/m	D_r/m	ΔP/bar	K	M	u_{max}/ms^{-1}	$\Delta T^{\circ}C$ max/min	$\Delta\theta_{film}$/°C max/min	T_i(max)/°C
0.05	0.05	18.1	0.268	0.113	602	$^{382}/_{283}$	$^{35.9}/_{21.3}$	718
0.075	0.05	16.9	0.250	0.235	602	$^{503}/_{249}$	$^{63.8}/_{17.6}$	867
0.10	0.05	16.8	0.247	0.290	602	$^{561}/_{241}$	$^{77.7}/_{16.8}$	939
0.05	0.075	5.01	0.074	0.161	382	$^{468}/_{285}$	$^{52.7}/_{22.3}$	821
0.075	0.075	4.01	0.059	0.059	267	$^{350}/_{305}$	$^{32.9}/_{25.5}$	714
0.10	0.075	3.85	0.057	0.086	267	$^{375}/_{297}$	$^{37.0}/_{24.4}$	713
0.05	0.10	2.97	0.044	0.186	382	$^{490}/_{272}$	$^{57.6}/_{20.4}$	848
0.075	0.10	1.95	0.029	0.047	151	$^{362}/_{316}$	$^{34.8}/_{27.3}$	697
0.10	0.10	1.79	0.026	0.027	151	$^{399}/_{319}$	$^{31.2}/_{27.8}$	670
0.20	0.10	1.72	0.025	0.040	151	$^{350}/_{315}$	$^{33.1}/_{27.3}$	683
0.05	0.20	2.05	0.030	0.199	382	$^{503}/_{267}$	$^{60.3}/_{19.6}$	863
0.10	0.20	0.91	0.013	0.021	96	$^{343}/_{322}$	$^{31.7}/_{28.4}$	675
0.20	0.20	0.84	0.012	0.002	38	$^{331}/_{329}$	$^{29.8}/_{29.6}$	661
0.075	0.25	1.03	0.015	0.062	267	$^{370}/_{306}$	$^{36.2}/_{25.9}$	706
0.20	0.25	0.81	0.012	0.001	24	$^{331}/_{330}$	$^{29.8}/_{29.6}$	661
0.25	0.25	0.80	0.012	0.001	24	$^{330}/_{330}$	$^{29.7}/_{29.6}$	660

TABLE 2

Calculated performance for a five-cell row: Effect of changing d_i

	d_i/m	D_s/m	D_r/m	ΔP/bar	K	P/bar	
	0.015	0.15	0.15	2.17	0.021	89.1	
A	0.015	0.20	0.20	2.08	0.021	89.1	Advantage taken of increase in allowable pressure
	0.015	0.25	0.25	2.05	0.020	89.1	
	0.015	0.15	0.15	3.24	0.047	59.8	
B	0.015	0.20	0.20	3.10	0.045	59.8	Pressure same as for d_i = 0.02m - set C
	0.015	0.25	0.25	3.06	0.045	59.8	
	0.02	0.15	0.15	0.97	0.015	59.8	
C	0.02	0.20	0.20	0.84	0.012	59.8	Compare set B
	0.02	0.25	0.25	0.80	0.012	59.8	
	0.025	0.15	0.15	0.66	0.014	42.0	
D	0.025	0.20	0.20	0.48	0.010	42.0	Sets A - D are for stainless steel ducts
	0.025	0.25	0.25	0.42	0.009	42.0	
	0.025	0.15	0.15	0.47	0.007	59.8	
E	0.025	0.20	0.20	0.34	0.005	59.8	Use of TZM or Inconel. P Limited by compressor
	0.025	0.25	0.25	0.30	0.005	59.8	

TABLE 3

Calculation of performance of a five-cell row: Effect of changing duct layout

D_s/m	D_r/m	ΔP/bar	K	M	T_i(max)/°C	
0.05	0.05	18.1	0.268	0.113	718	Original layout as in Figure 12
0.15	0.15	0.98	0.015	0.006	662	
0.20	0.20	0.84	0.013	0.002	661	
0.05	0.05	16.2	0.223	0.750	1176	Layout (i) in Figure 15
0.15	0.15	0.99	0.015	0.026	676	
0.20	0.20	0.84	0.013	0.007	664	
0.05	0.05	11.9	0.179	0.920	1258	Layout (ii) in Figure 15
0.15	0.15	0.99	0.015	0.037	670	
0.20	0.20	0.84	0.013	0.012	665	

TABLE 4

Calculation of performance of a three-cell row

D_s/m	D_r/m	ΔP/bar	K	M	$T_{i(max)}$/°C
0.05	0.05	7.22	0.105	0.147	738
0.10	0.10	1.17	0.017	0.020	667
0.25	0.10	1.12	0.017	0.021	669
0.20	0.20	0.80	0.012	0.001	661
0.10	0.25	0.83	0.012	0.012	665
0.25	0.25	0.79	0.012	0.001	660

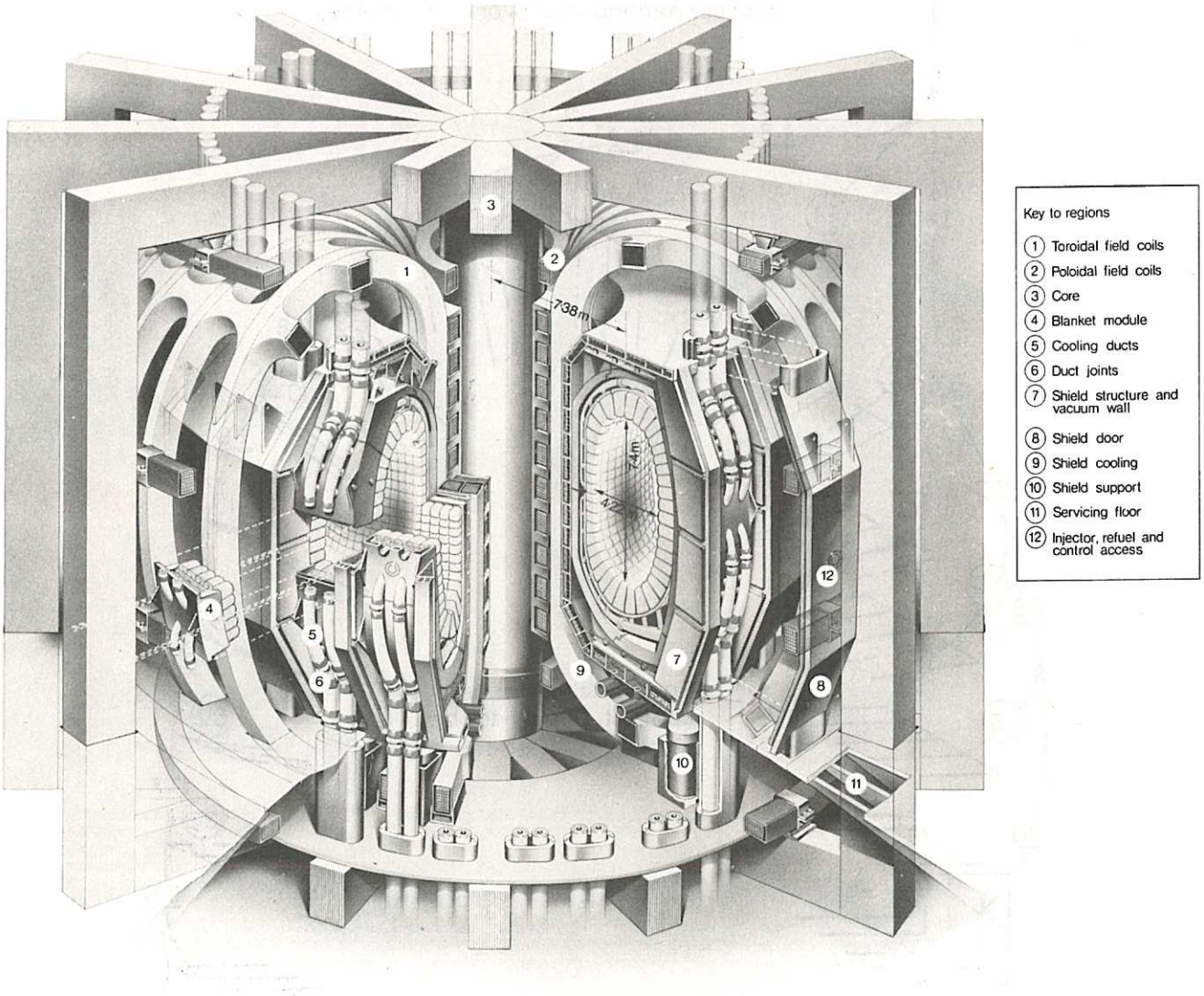

Fig.1 Artist's impression of the Culham Conceptual Tokamak Reactor Mk IIA. The principal dimensions are given on the vertical section on the right hand side. The left side shows nearest the centre a segment with the top half removed and adjacent, a sub-module in space. Both illustrate the arrangement of the blanket cells in horizontal rows.

CLM-P572

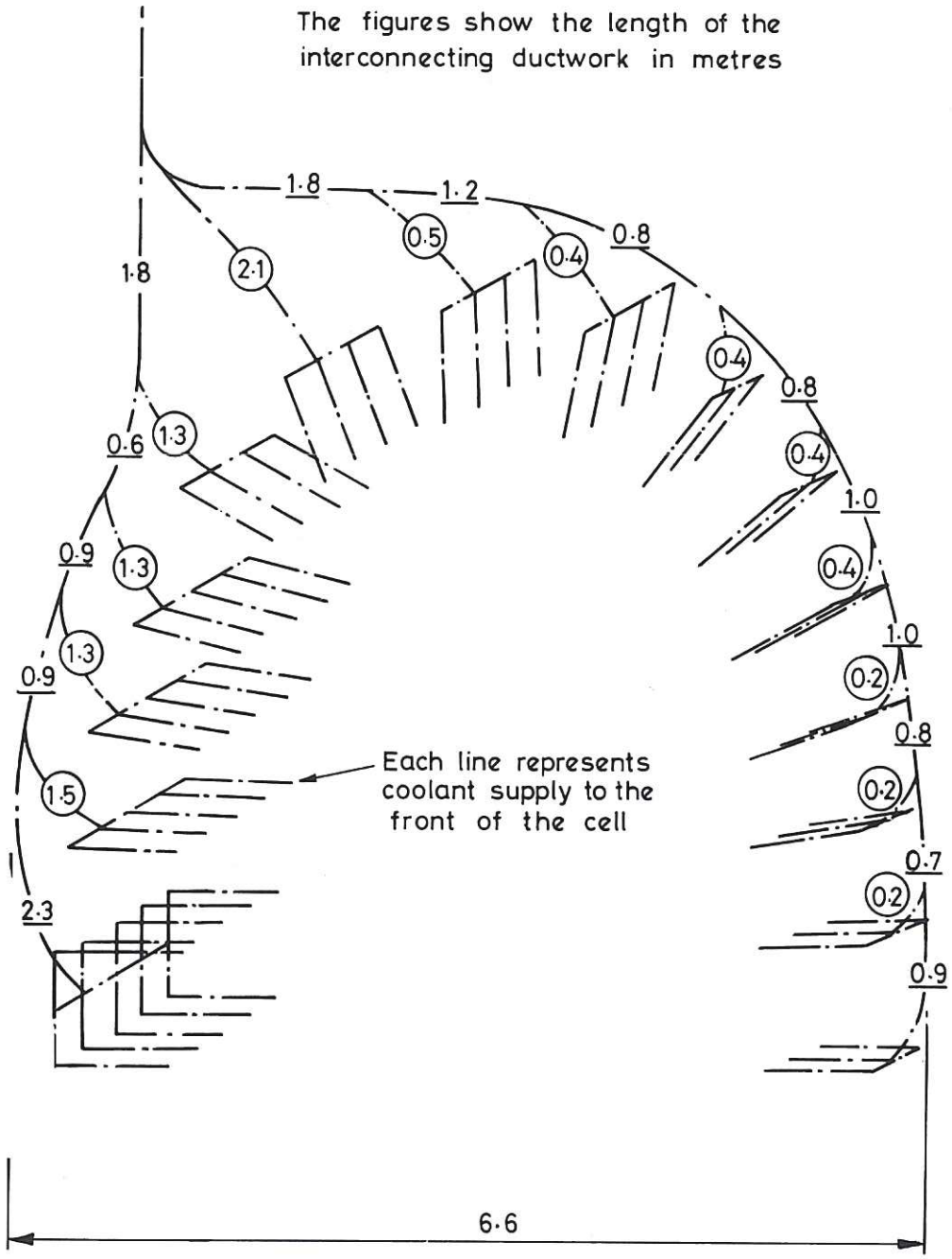

Fig.2 Layout of ducts in CCTR-II.

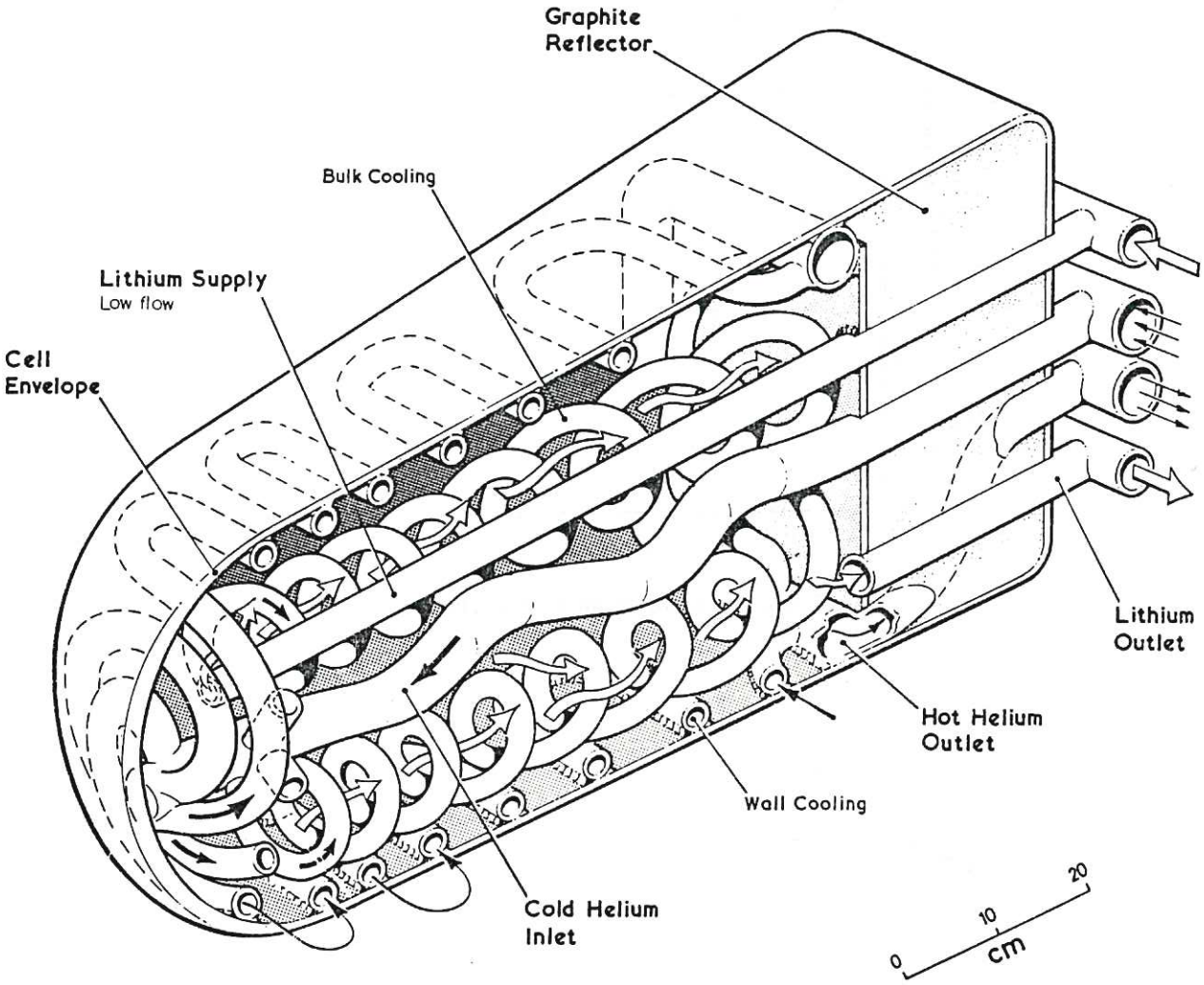

Fig.3 Proposed helium cooled blanket cell, Mitchell and Booth [4].

CLM-P572

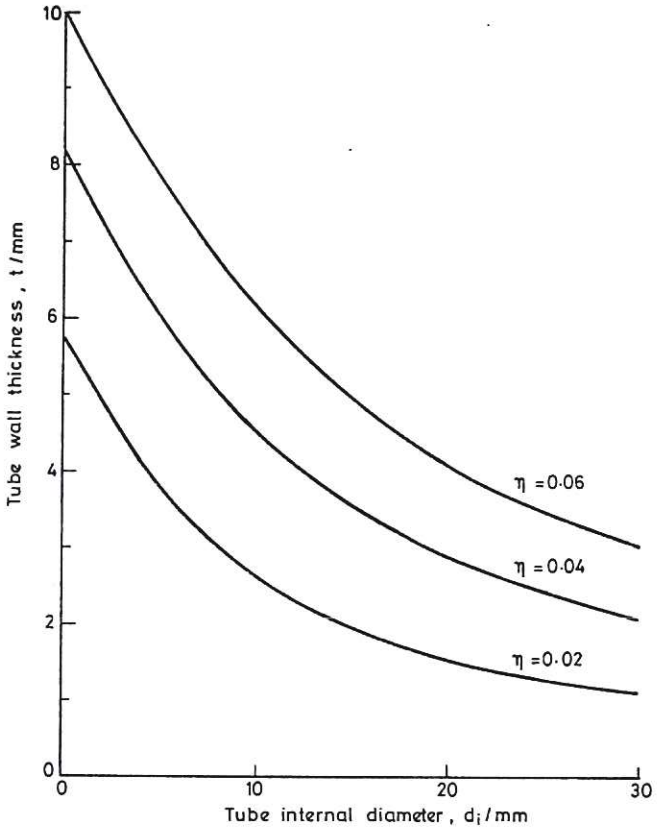

Fig.4 Plot of t against d_i for various values of η.

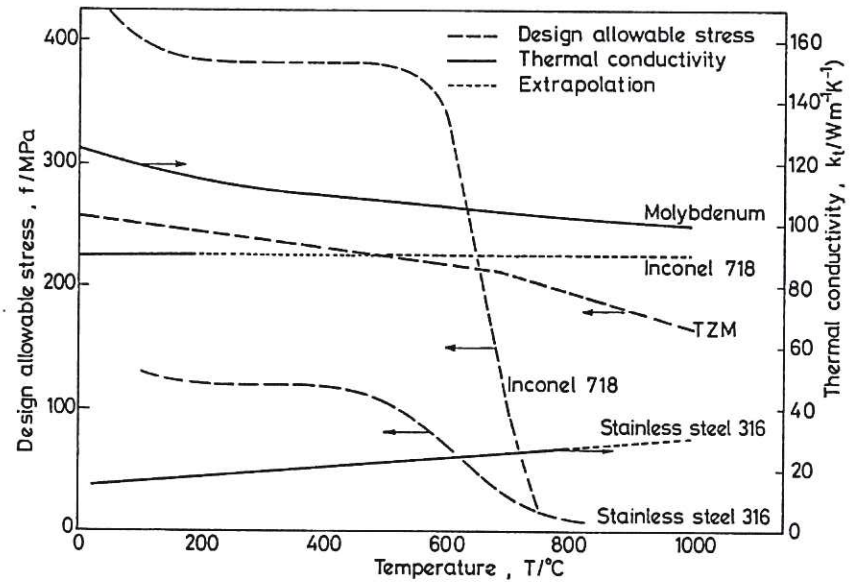

Fig.5 Design allowable stresses and thermal conductivities of possible duct materials in CCTR-II.

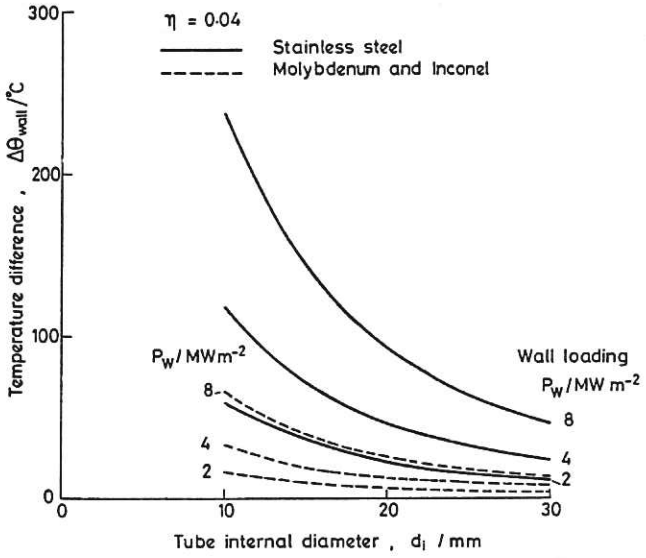

Fig.6 Temperature difference across cell coolant tubes for various construction materials and wall loadings.

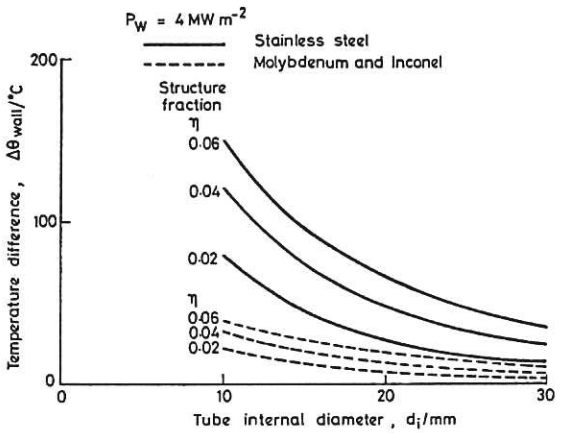

Fig.7 Temperature difference across cell coolant tubes for various construction materials and structure fractions.

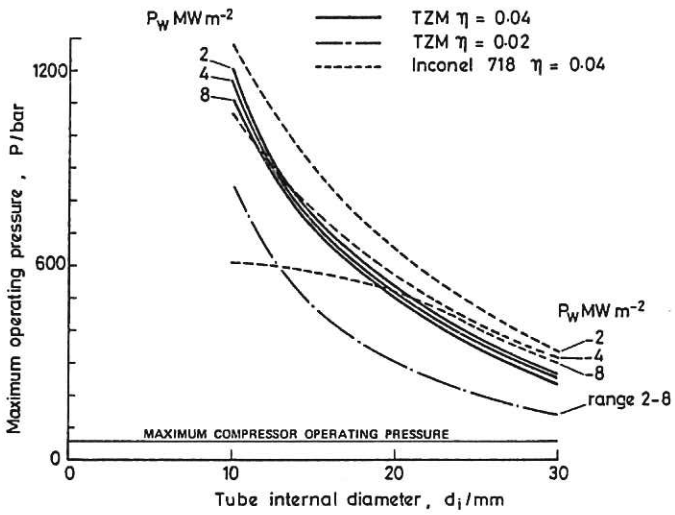

Fig.8 Maximum operating pressures for TZM and Inconel 718 defined by working stress limits.

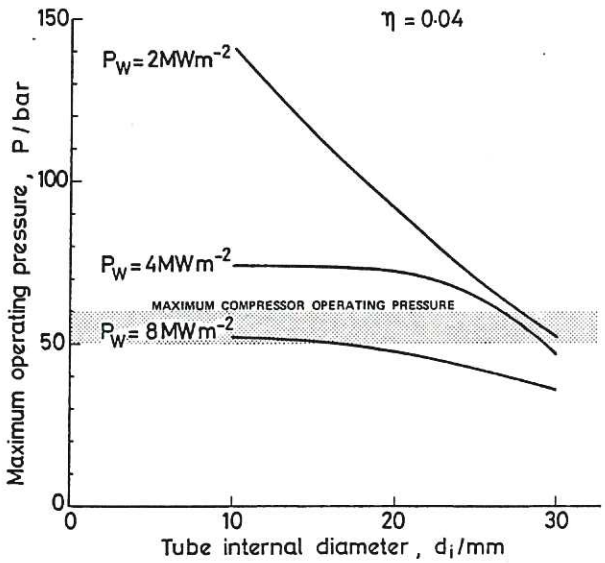

Fig.9 Maximum operating pressures for stainless steel defined by working stress limits.

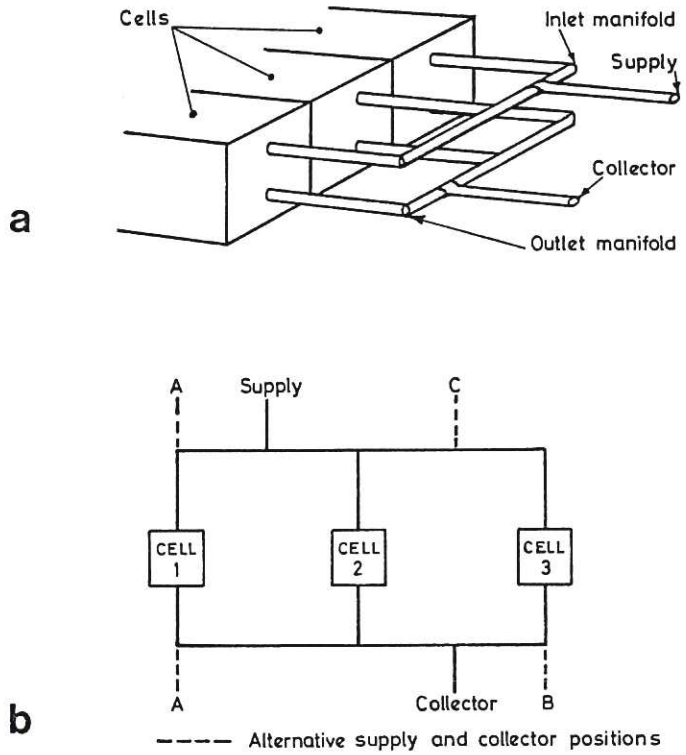

Fig.10 Ducting in blanket cell rows. (10a) Illustration of blanket cell row and interconnecting ducts. (10b) Diagrammatic representation of Fig.10a showing alternate layouts.

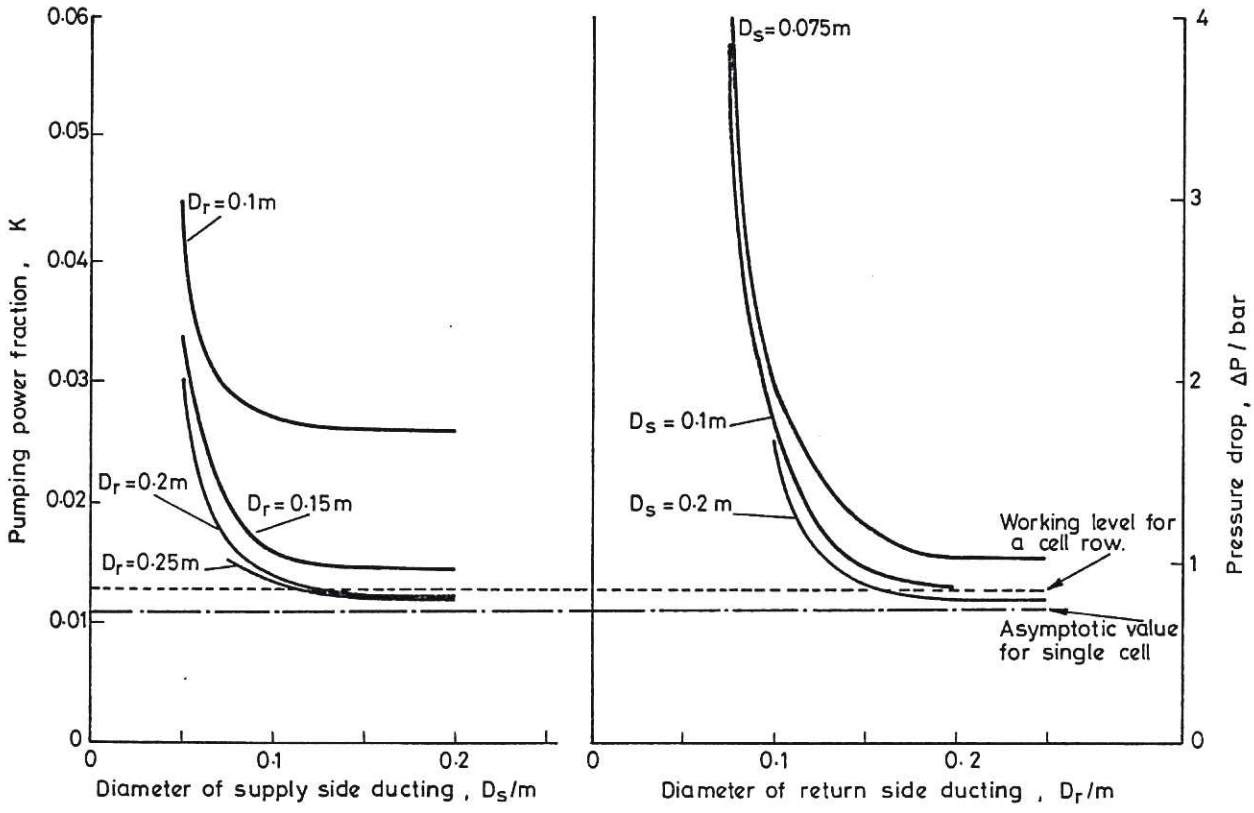

Fig.11 Effect of ducting diameter on pressure loss and pumping power fraction in a 5-cell row.

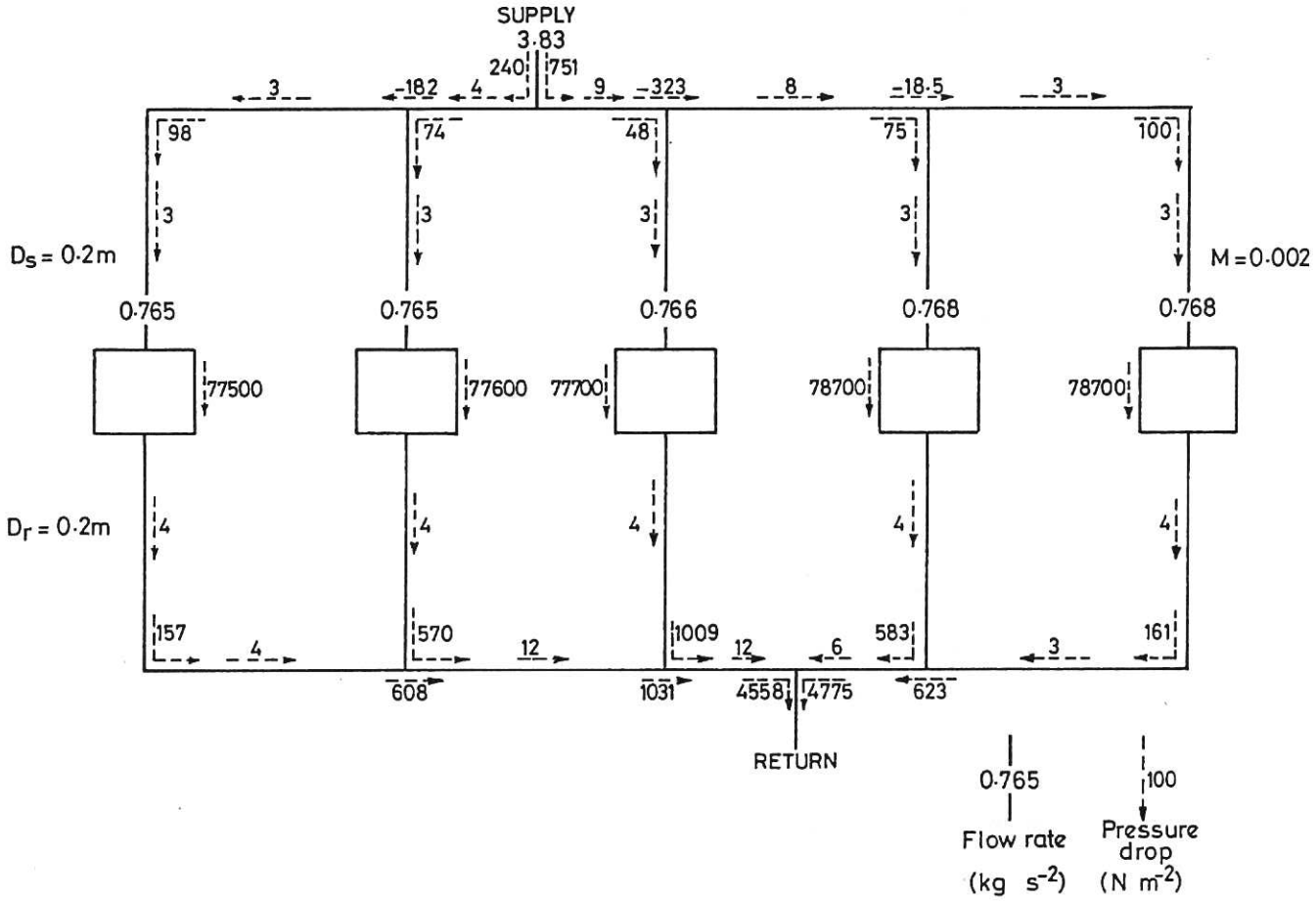

Fig.12 Detailed analysis of flow distribution in a 5-cell row, with 0·2m bore ducting.

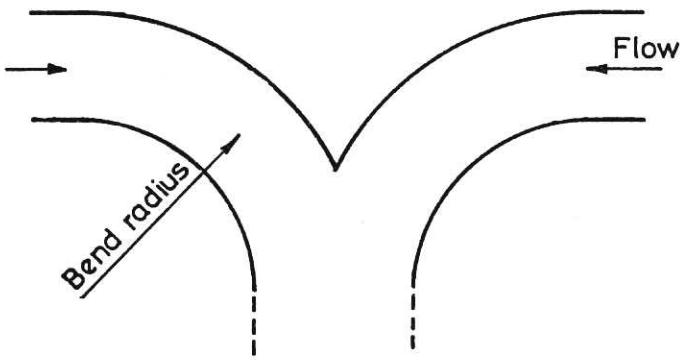

Fig.13 Rounded junction for reduction of pressure loss.

CLM-P572

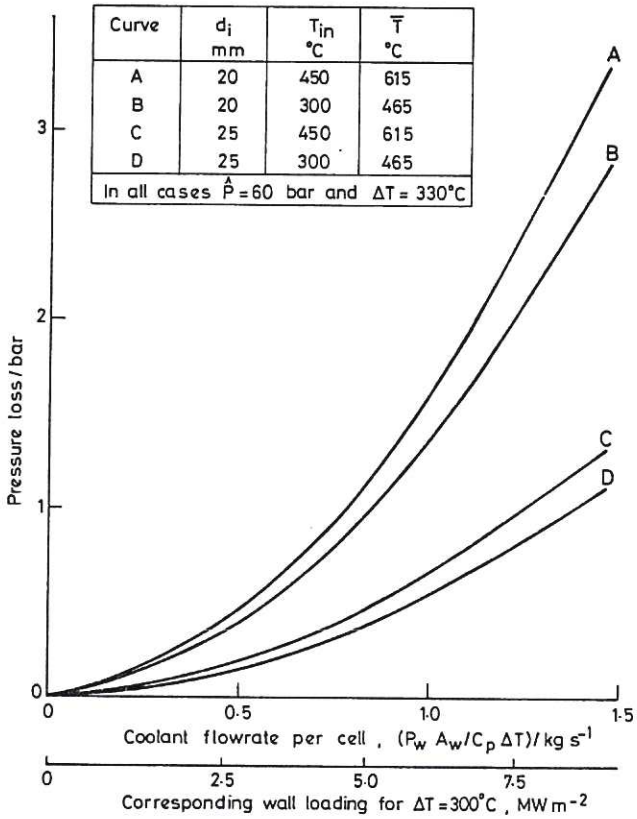

Fig.14 Plot of pressure loss in a 5-cell row against coolant flow rate, effect of d_i and $\bar{T}$.

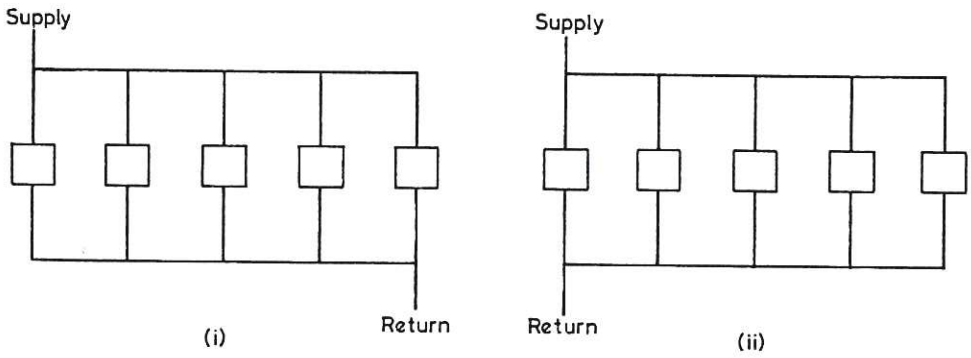

Fig.15 Alternate ducting layouts for a 5-cell row.

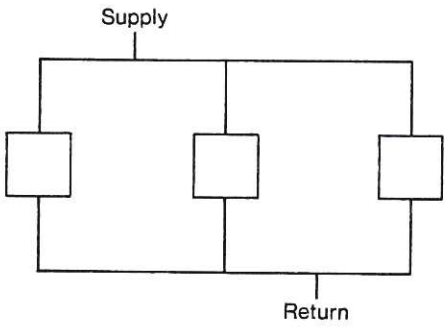

Fig.16 Layout of ducting for a 3-cell row.

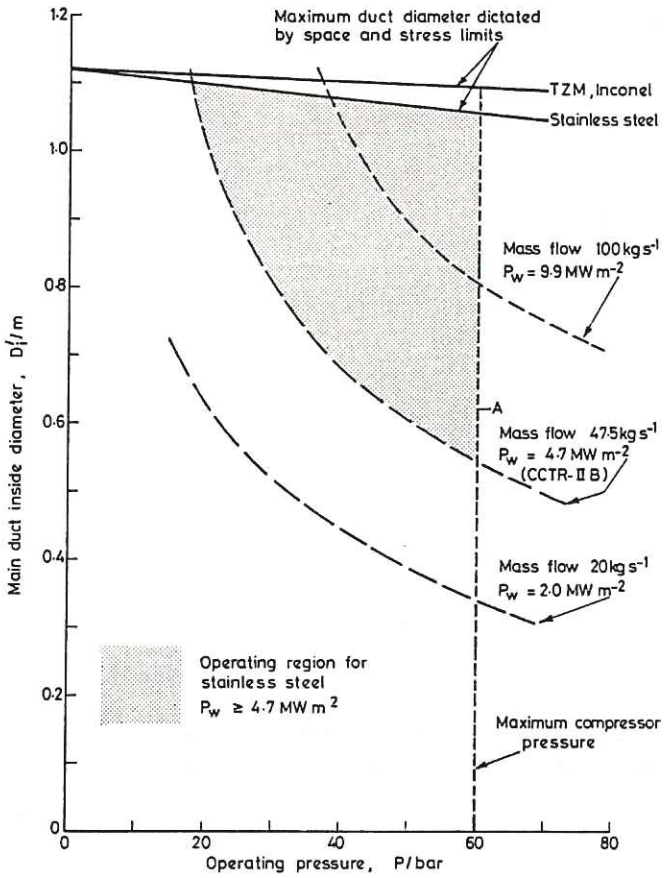

Fig. 17 Size limitations of main cooling ducts. The three curves show the minimum duct diameter versus pressure for three values of wall loading P_W.

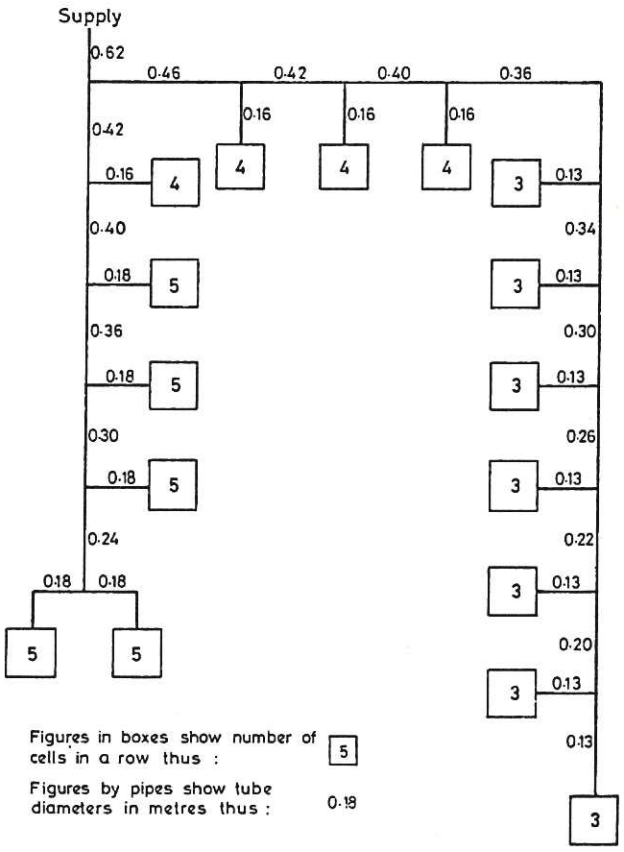

Fig.18 Simplified flow sheet of half segment.

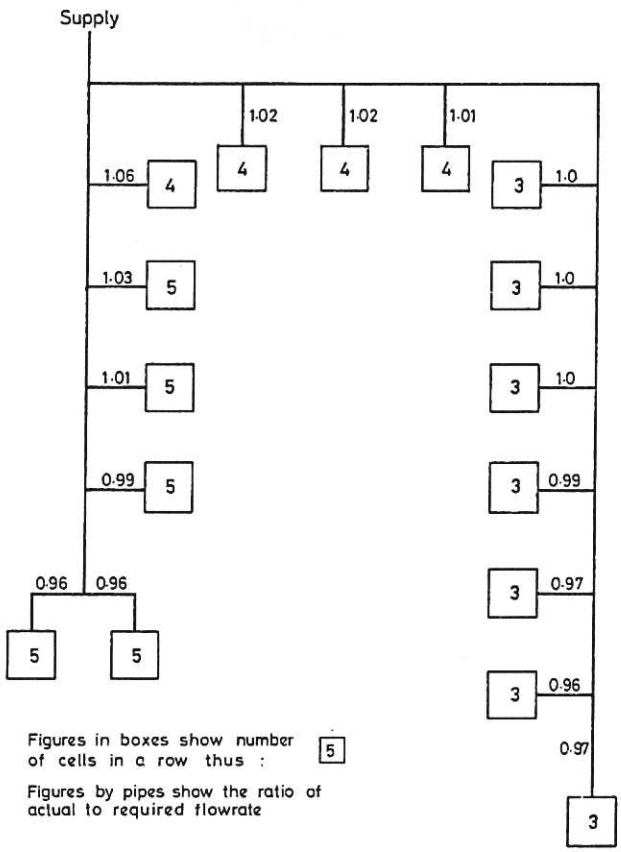

Fig.19 Flow distribution in a half segment.

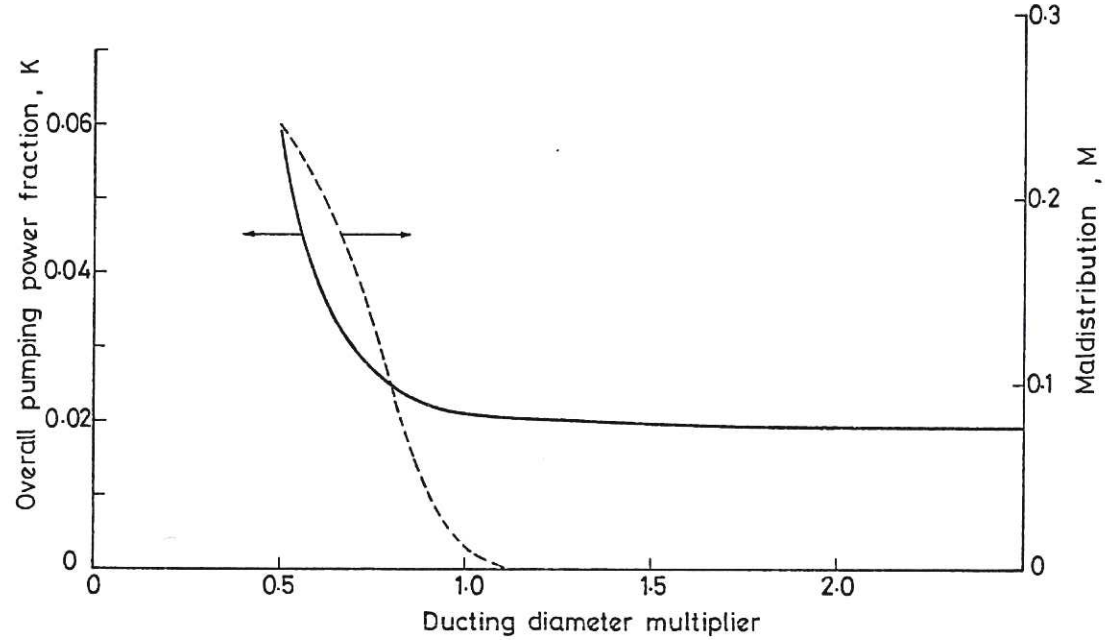

Fig.20 Effect of ducting diameter on pumping power fraction and maldistribution in a complete coolant circuit.

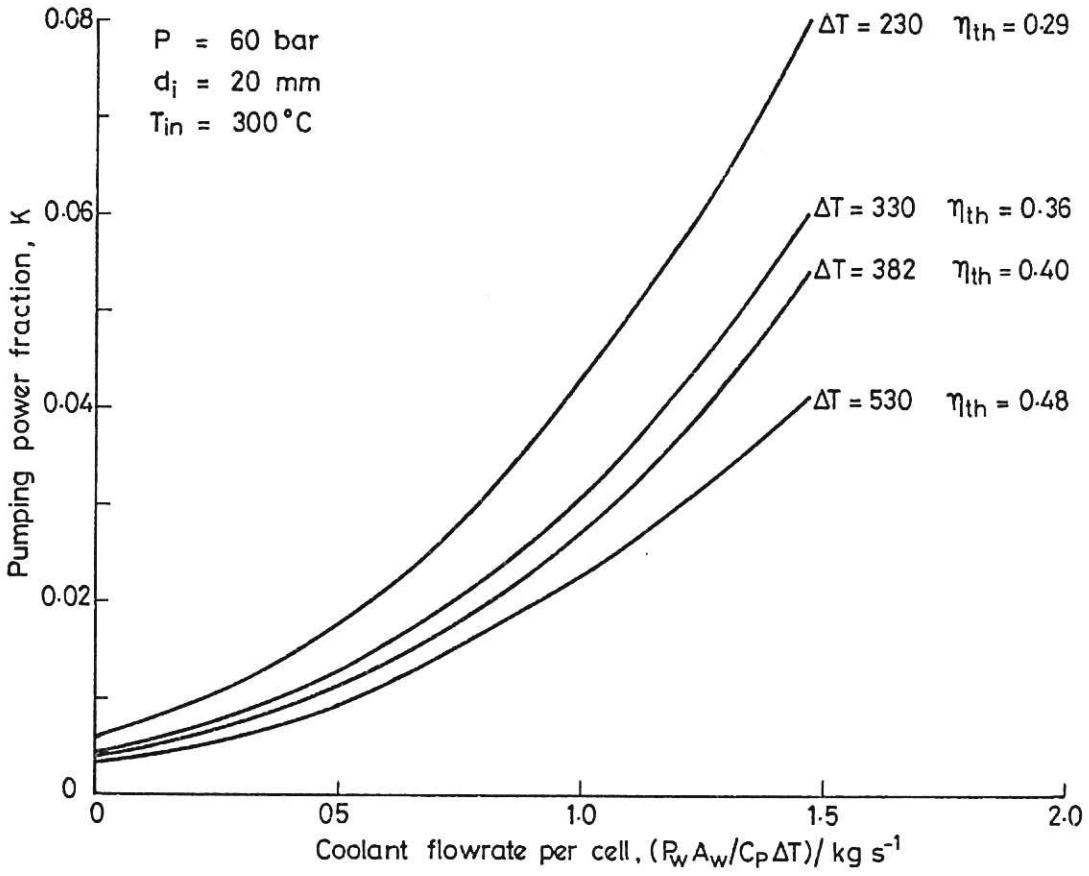

Fig.21 Plot of overall pumping power fraction against coolant flow rate for various thermodynamic efficiencies.

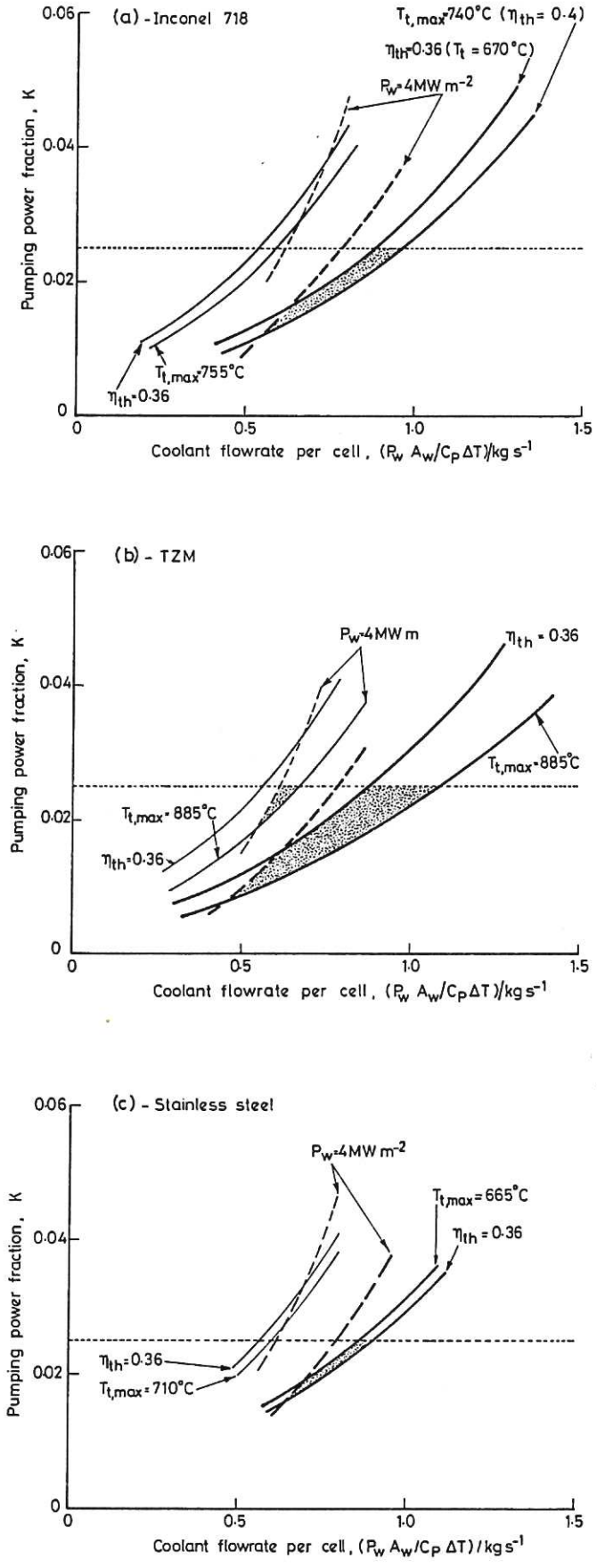

Fig.22 Design option regions. The thick and thin curves are for coolant pressures of 60 and 40 bar respectively. The dashed curves give the minimum coolant flow for 4MW m^{-2} wall loading for the two coolant pressures.

CLM-P572

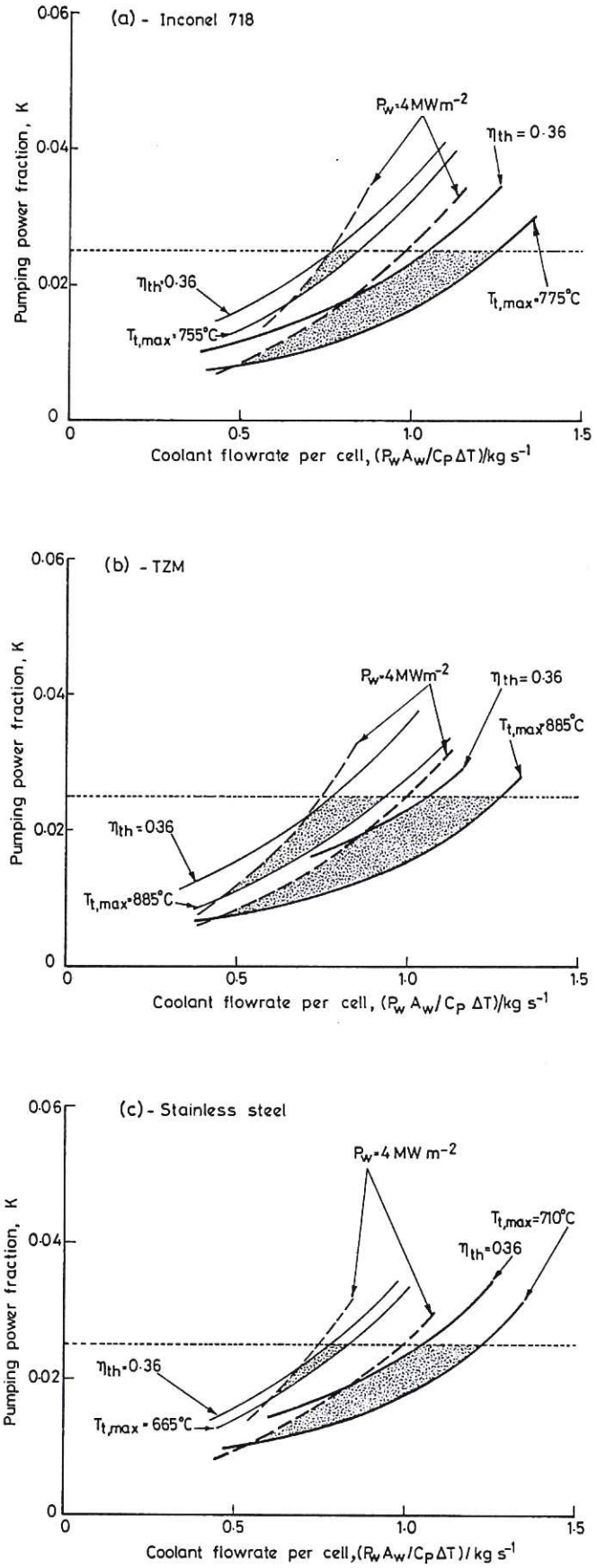

Fig.23 Design option regions. The thick curves are for P = 60 bar, d_i = 20mm, T_{in} = 200°C, the thin curves are for P = 40 bar, d_i = 25mm, T_{in} = 300°C. The dashed curves give the minimum coolant flow for 4MW m^{-2} wall loading for the two sets of conditions.

(a) Blanket cells

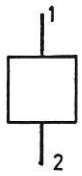

(b) Straight lines.

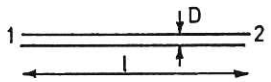

(c) Dividing flow. (Type 1) arrows indicate direction of flow

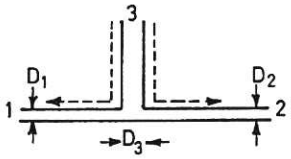

(d) Dividing flow. (Type 2)

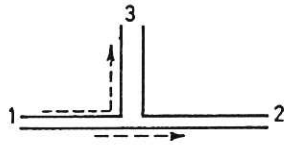

(e) Joining flow. (Type 1)

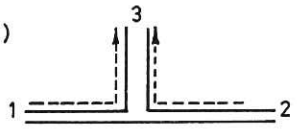

(f) Joining flow (Type 2)

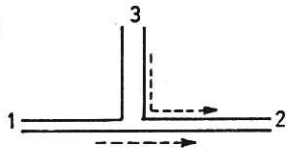

Fig.A1 Configurations of cell row units.

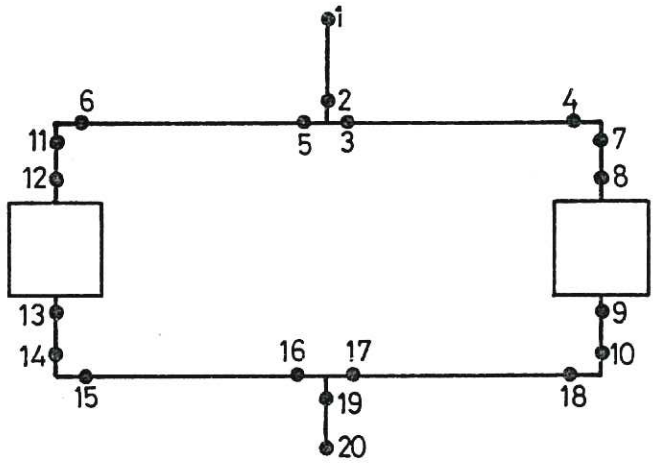

Fig.A2 Example of node numbering for complex piping networks.